

The Value of Summary Statistics for Anomaly Detection in Temporally-Evolving Networks: A Performance Evaluation Study

Lata Kodali*, Srijan Sengupta, Leanna House, William H. Woodall

Abstract

Analysis of network data has emerged as an active research area in statistics. Much of the focus of ongoing research has been on static networks that represent a single snapshot or aggregated historical data unchanging over time. However, most networks result from temporally-evolving systems that exhibit intrinsic dynamic behavior. Monitoring such temporally-varying networks to detect anomalous changes has applications in both social and physical sciences. In this work, we perform an evaluation study of the use of summary statistics for anomaly detection in temporally-evolving networks by incorporating principles from statistical process monitoring. In contrast to previous studies, we deliberately incorporate temporal auto-correlation in our study. Other considerations in our comprehensive assessment include types and duration of anomaly, model type, and sparsity in temporally-evolving networks. We conclude that the use of summary statistics can be valuable tools for network monitoring and often perform better than more complicated statistics.

1 Introduction

Recent decades have witnessed an explosion of data in the form of networks, representing important systems in various fields, e.g., physical infrastructure (Huberman and Adamic, 1999; Pagani and Aiello, 2013), social interaction (Milgram, 1967; Adamic and Glance, 2005), and biological systems (Bassett and Bullmore, 2006; Lynall et al., 2010). Consequently, statistical modeling and analysis have become fundamental tools for studying physical and virtual networked systems, and are poised to become even more critical in the near future.

Traditionally, most research has focused on static modeling of networks, in which either a single snapshot or aggregated historical data of a system are available. However, usually networks result from time-evolving systems that exhibit intrinsic dynamic behavior. The terms dynamic, temporally-evolving, time-evolving, or temporally dependent are all used interchangeably to describe such networks that span over time. For example, often the relationships between members of a social network evolve over time due to finding new friends, collaborating with new colleagues, moving to another department, etc. Recent studies have focused on analyzing dynamic networks where a network is represented by a statistical/probabilistic model that is adaptively updated over time. However, many of these models have been developed on the premise that a system either is stationary or has smooth dynamics, and it does not experience abrupt changes.

In applications, the occurrence of sudden large changes and shocks in time-varying networks is very common. For example, resignation of a key employee or occurrence of a conflict in an

*Contact Email: latak215@vt.edu

organization may cause a significant change in the professional network of the employees. As another example, the occurrence of a change in the communications network of a terrorist group may indicate a high possibility of a terrorist attack that could be prevented if the change is detected quickly. Similarly, significant changes in the brain connectome network (Xia et al., 2013) of an individual can indicate the onset of a neurological disorder like Alzheimer’s disease or epilepsy. Monitoring, change detection, and accurate estimation of the change time are crucial for effective decision-making and for taking necessary actions in a timely manner. Moreover, abrupt changes often affect a network locally. That is, only a subset of nodes and their corresponding links are altered by an event. Consequently, diagnosis, defined as identifying affected sub-networks, plays an important role in root-cause determination and action planning. For example, it is crucial to determine the group of people who might be involved in a terrorist plot, or the parts of the brain involved in a particular disease, by identifying the set of nodes that caused the change in the corresponding network.

A recent review paper by Woodall et al. (2017) provides an assessment of monitoring methods that may detect anomalies in time-evolving networks. Specifically, they reviewed statistical process monitoring methods for social, dynamic networks which fall into five broad categories: hypothesis testing (signals based on likelihood ratio tests), Bayesian methods (control limits are calculated using a Bayesian predictive distribution), scan methods (signals from a moving window based monitoring statistic), time series models (signals from large residuals), and changes in community structures/membership. While summarizing the categories, Woodall et al. (2017) highlight differences among available methods for specifying tuning parameters, such as specifying the size of moving average window, defining control limits based on baseline data, and approaches for removing seasonal effects in data. A notable point made by Woodall et al. (2017), which was re-iterated in Sengupta and Woodall (2018), is that even with variation in parameter settings comparable relevant work in the literature are not available for detecting abrupt changes in a stream of time-varying networks. Similarly, several papers contain studies of network monitoring under specific parametric modeling frameworks (Wilson et al., 2019; Yu et al., 2018; Zhao et al., 2018a,b). However, such monitoring methods work under the assumption of a specific network model, and cannot be extended to the general task of network monitoring without model assumptions.

In this paper, we assess the performance of model-free summary statistics in network monitoring, such as network density, maximum degree, and their linear combinations, in anomaly detection. Such summary statistics are simple to calculate and often used in practice, but little is understood about how these summary statistics behave under varying network conditions and over time. In turn, the utility of common network summaries, such as density and maximum degree, for anomaly detection is also currently unclear. For our work, we conduct a comprehensive simulation study to assess both the successes and failures of four monitoring statistics that are functions of network density and/or maximum degree in comparison to a well-studied scan-based moving window approach (Priebe et al., 2005). We measure success and failure for the methods based on false alarm rates, anomaly detection rates, and Area Under Curve (AUC) calculations from receiver operating characteristic (ROC) curves.

An important aspect of our work is in applying monitoring methods on temporally dependent network data to evaluate method performance in realistic scenarios. The data are simulated from well-studied network models so that we may introduce various kinds of anomalies in a controlled manner to facilitate a principled comparative evaluation of network monitoring methods. As pointed out by several authors (Woodall et al., 2017; Savage et al., 2014; Azarnoush et al., 2016),

compared to case studies, such controlled scenarios from synthetic networks provide a more principled testbed for performance assessment.

The remainder of the paper is as follows. The anomaly detection methods utilized, mathematical formulas, and considerations for such methods utilized are given in Section 2. In order to better understand what types of anomalies can be detected, the network monitoring methods were applied to data generated from two popular latent variable models: the dynamic latent space model (DLSM) (Sewell and Chen, 2015) and the dynamic degree-corrected stochastic block model (DD-CSBM) (Wilson et al., 2019; Matias and Miele, 2017). Brief overviews of these models are given in Section 3. We reiterate that no model fitting occurred and models were only used to generate data of temporally-evolving networks. A performance evaluation of network monitoring methods on summary statistics is accomplished using a comprehensive simulation study. Settings for the simulation study as well as planted anomalies are discussed in Section 4. Lastly, we summarize our findings and discuss future work in Section 5.

2 Summary Statistics and Network Monitoring Methods

For anomaly detection, we discuss which statistics are monitored and methods by which to monitor these statistics. The summary statistics calculated from network data and interpretations of such quantities in a network are described in Section 2.1. How common techniques used in statistical process monitoring are applied to network data is described in Section 2.2. Threshold decisions for the selected monitoring approaches are further discussed in the evaluation of monitoring approaches in Section 4.

2.1 Summary Statistics

We first define our mathematical notation. Let n represent the number of nodes in a network at time t , where t evolves discretely until time T . Let \mathbf{Y}_t represent an adjacency matrix at time $t \in \{1, 2, \dots, T\}$ and y_{ijt} represent an edge weight at time t between nodes i and j , for $i, j \in \{1, 2, \dots, n\}$.

Density is defined as the sum of edges in a network divided by its total number of possible edges at time t . For n nodes, the total number of possible edges is $\binom{n}{2} = \frac{n(n-1)}{2}$, and for \mathbf{Y}_t , the sum of all edges at time t is $\sum_{i=1}^n \sum_{j=1; j \neq i}^n y_{ijt}$. If we let W_t represent density at time t , then

$$W_t = \frac{2}{n(n-1)} \sum_{i=1}^n \sum_{j=1; j \neq i}^n y_{ijt}. \quad (1)$$

Density is considered to be a global measure of a network; a measure that describes the entire network.

A local measure of a network might summarize individual nodes, such as degree. Let D_{it} represent the degree of node i within a network at time t . In a directed network, $D_{it} = \sum_{j=1}^n (y_{ijt} + y_{jit})$; D_{it} is the sum of in- and out-degrees within directed networks. For undirected networks, one divides D_{it} in half. To form a global measure from the local node degrees, **maximum degree** is often reported. Let D_t represent the maximum degree of a network at time t ;

$$D_t = \max_i \{D_{it}\}. \quad (2)$$

For this paper, we monitor network density, maximum degree, and **two linear combinations of density and maximum degree**, denoted M_t^- and M_t^+ . We define M_t^- and M_t^+ as follows:

$$M_t^- = \frac{1}{n}D_t - W_t \quad (3)$$

$$M_t^+ = \frac{1}{n}D_t + W_t. \quad (4)$$

We compare the effectiveness of monitoring W_t , D_t , M_t^- , and M_t^+ to detect anomalies relative to each other and a scan statistic, S_t^* , that was proposed by Priebe et al. (2005). Calculations for S_t^* result over moving windows of size m (e.g., $m=20$) over time t ($t \in \{2m+1, \dots, T\}$) and are based on the size of local neighborhoods of each node i . Neighborhoods within a network at time t are determined from a pre-specified order k , e.g., $k = \{0, 1, 2\}$ in that each neighborhood i ($i \in \{1, 2, \dots, n\}$) is the set of all nodes (and edges between them) within k edges of node i . Thus, the size of an order k neighborhood is the number of edges contained in that neighborhood. Let $O_{i,t}^{(k)}$ denote the size of an order k neighborhood of i and time t . Note, when $k = 0$, the size of an order 0 neighborhood is equivalent to degree. The calculated scan statistic for order k with moving window m involves a 2-step process on the sizes of order $k = \{0, 1, 2\}$ neighborhoods (Zhao et al., 2018a). We represent scan statistics based on order k as $S_t^{*(k)}$, for $k = \{0, 1, 2\}$ and define $S_t^* = \max\{S_t^{*(0)}, S_t^{*(1)}, S_t^{*(2)}\}$ when reporting results.

We now overview this 2-step process as is explained in Zhao et al. (2018a) summarizing the work of Priebe et al. (2005). First step is to standardize $O_{i,t}^{(k)}$ using a previous window of size m . That is, the first standardization of $O_{i,t}^{(k)}$ with $t > m$ is calculated by

$$O_{i,t}^{*(k)} = \frac{O_{i,t}^{(k)} - \text{mean}(O_{i,t}^{(k)})}{\max(\text{sd}(O_{i,t}^{(k)}), 1)},$$

with

$$\text{mean}(O_{i,t}^{(k)}) = \frac{1}{m} \sum_{j=1}^m O_{i,t-j}^{(k)} \quad \text{and} \quad \text{sd}(O_{i,t}^{(k)}) = \sqrt{\frac{1}{m-1} \sum_{j=1}^m [O_{i,t-j}^{(k)} - \text{mean}(O_{i,t}^{(k)})]^2}$$

for $k = \{0, 1, 2\}$ and $i \in \{1, 2, \dots, n\}$. The lower bound of 1 in the denominator of $O_{i,t}^{*(k)}$ prevents detection of relatively small (perhaps too small) changes in a network. This first standardization of $O_{i,t}^{*(0)}$, $O_{i,t}^{*(1)}$, and $O_{i,t}^{*(2)}$ are done for all times $t > m$. The second step of the process involves standardizing the maxima of $O_{i,t}^{*(k)}$ across nodes i . Let $S_t^{(k)} = \max_i \{O_{1,t}^{*(k)}, O_{2,t}^{*(k)}, \dots, O_{n,t}^{*(k)}\}$ and calculate across nodes i and time $t > 2m$, $S_t^{(0)}$, $S_t^{(1)}$, and $S_t^{(2)}$. Then, the second standardization of $S_t^{*(k)}$ with $t > 2m$ is calculated by

$$S_t^{*(k)} = \frac{S_t^{(k)} - \text{mean}(S_t^{(k)})}{\max(\text{sd}(S_t^{(k)}), 1)}, \quad (5)$$

with

$$\text{mean}(S_t^{(k)}) = \frac{1}{m} \sum_{j=1}^m S_{t-j}^{(k)} \quad \text{and} \quad \text{sd}(S_t^{(k)}) = \sqrt{\frac{1}{m-1} \sum_{j=1}^m [S_{t-j}^{(k)} - \text{mean}(S_t^{(k)})]^2}$$

for $k = \{0, 1, 2\}$.

Finally, monitoring scan statistics, S_t^{*k} , begin at time $t = 2m + 1$ since the first $2m$ windows are needed to start the procedure. For more details on S_t^{*k} , see both Priebe et al. (2005) and Zhao et al. (2018a).

Table 1 provides a list of statistics that we study in this paper for network monitoring. We chose these statistics for their simplicity, popularity, flexibility, and relative meaning in dynamic networks. For example, network densities over time are easy to calculate and have the potential to reveal both global or local changes in networks. Globally, several nodes may increase or decrease communication (even slightly) over set time(s) in a network, and locally, a few nodes may significantly increase or decrease communication. Both such global and local changes could be reflected in changes of network densities. Note, “communication”, refers to the number or weight of edges in nodes. Similarly, maximum degree may capture global and local changes based on all or a set node behaviors. By combining measures of degree and density, e.g., with “Difference” (M_t^-) and “Sum” (M_t^+) statistics, there is additional opportunity to capture global and/or local changes in networks. For example, with binary networks where $y_{ijt} \in \{0, 1\}$, we know $D_t \leq n$ and $D_t/n \leq 1$. Thus, $M_t^- = (\frac{1}{n}D_t - W_t) \leq 1$, because $0 \leq W_t \leq 1$. When M_t^- values are high (close to 1) there is large discrepancy between network density and the average node degree. This would suggest that individual nodes may be highly connected with other nodes (local behavior), while the overall communication of other nodes is scarce (global behavior). Finally, the scan method S_t^* is popular and well-cited, thus it makes sense to ground our analyses of four summary statistics by its performance. However, the scan statistic is harder to calculate than the other statistics that we study. Furthermore, for large-scale networks (e.g., social media) and real-time monitoring, computing the scan statistic can be computationally expensive and/or infeasible. Thus, in addition to comparing the effectiveness of five common network summaries, we may form opinions on the trade-offs between complex and simple monitoring approaches.

Name (at time t)	Notation
Density	W_t
Max Degree	D_t
Difference	M_t^-
Sum	M_t^+
Scan Statistic	S_t^*

Table 1: Summary statistics for dynamic networks: complexity increases from top to bottom.

2.2 Statistical process monitoring for networks

Statistical process monitoring is a well-studied area, but applying these techniques to network data is not straightforward; e.g., it is unclear how to set control limits for network data. The general network monitoring approaches are discussed in Section 2.2 while considerations for control limits are further discussed in Sections 2.2.1 and 2.2.2.

The summary statistics calculated are monitored in two ways. One way utilizes a control chart described in Algorithm 1, and the other utilizes a moving window approach over-viewed in Algorithm 2. In the first approach, there are three main steps. Step one, establish T_1 , the number of time-points required to determine baseline behavior of a network. We refer to data from $t = 1$

through $t = T_1$ as Phase I data, where network snapshots are assumed to have no anomalies. Next, after establishing Phase I data, appropriate control limits, i.e., thresholds for expected non-anomalous behavior, must be determined. Third, established control limits from Phase I data are applied to remaining time-points, i.e., $t > T_1$, called Phase II data, in order to detect any anomalies or atypical behavior.

Similar to the first approach, the second approach has three main steps. First, a moving window approach requires a window length, m , to be set, e.g. 20 time-points. Specifically for the scan statistic, in addition to the first set of m time-points, yet another set of m time-points is needed to start the method. Second, a threshold must be determined for acceptable behavior. Third, the remaining moving windows of length m are observed using that threshold. In both approaches, whether or not an anomaly occurred is recorded using $\mathbf{A} = \{A_1, A_2, \dots, A_{T-T_1}\}$ such that $A_t = 1$ when an anomaly is detected and 0 otherwise.

We exemplify the two approaches on M_t^- and S_t^* in Figure 1. From Figure 1 (a), we observe control limits, $CL = \hat{\mu} \pm q\hat{\sigma}$, are calculated using Phase I data, and likewise from Figure 1 (b), we see the monitoring process begin at time 41 when using window size $m = 20$ with an acceptable threshold for the scan statistic. In this illustration, both methods signal around time-point 60.

In the first monitoring approach, Shewhart individual control charts are utilized for a majority of our summary statistics. In any control chart, a statistic is observed over time with control limits indicating expected behavior of that statistic. Since the network data are *correlated snapshots* over time, control limits should be adjusted for such correlation. Control limits of a Shewhart individuals control chart are $\bar{x} \pm (3\overline{MR})/d_2$ where d_2 is an anti-biasing constant and set to 1.13; and MR is a moving range, for a process $\{x_1, x_2, \dots, x_n\}$ so that $MR = |x_i - x_{i-1}|$ ($i > 1$) (Montgomery, 2007). However, in the context of network data, these control limits may not be appropriate. In Section 2.2.1, we assess whether the standard deviation of our summary statistics is appropriately measured using \overline{MR}/d_2 , and in Section 2.2.2, we evaluate the utility of applying 3 times the standard deviation as control limits.

Algorithm 1 General Monitoring Approach for W_t , D_t , M_t^- , and M_t^+ .

Input: Temporally-evolving network data.

Output: $\mathbf{A} = \{A_{T_1+1}, A_{T_1+2}, \dots, A_T\}$ where $A_t = 1$ if anomaly is detected at time t and 0 otherwise.

- 1: Set number of time-points for Phase I data, T_1 . Data from Phase I is assumed to be non-anomalous.
- 2: Use Phase I data to determine control limits for a Shewhart individuals control chart. Control limits (CL) are of the form: $CL = \hat{\mu} \pm q\hat{\sigma}$.
- 3: **For** t **in** $(T_1 + 1) : T$ **{**

For a summary statistic at time t , denoted x_t , record if an anomaly occurred or not using:

$$A_t = \begin{cases} 1, & x_t < \hat{\mu} - q\hat{\sigma} \\ 1, & x_t > \hat{\mu} + q\hat{\sigma} \\ 0, & \text{otherwise} \end{cases}.$$

} **END**

Algorithm 2 General Monitoring Approach for S_t^* .

Input: Temporally-evolving network data.

Output: $\mathbf{A} = \{A_{T_1+1}, A_{T_1+2}, \dots, A_T\}$ where $A_t = 1$ if anomaly is detected at time t and 0 otherwise.

- 1: Determine the length of moving window, i.e. set number of time-points for a window, m .
- 2: Use $2m$ windows for starting the scan method. First set of m windows is for maximizing across nodes. Second set of m windows is for maximizing across time.
- 3: Set threshold, q , to determine if an anomaly occurred or not, where $q \in \{1, 2, 3, \dots\}$.
- 4: **For** t **in** $(T_1 + 1) : T$ **{**

For scan statistic at time t , denoted S_t^* , record if an anomaly occurred or not using:

$$A_t = \begin{cases} 1, & S_t^* > q \\ 0, & \text{otherwise} \end{cases}.$$

} END

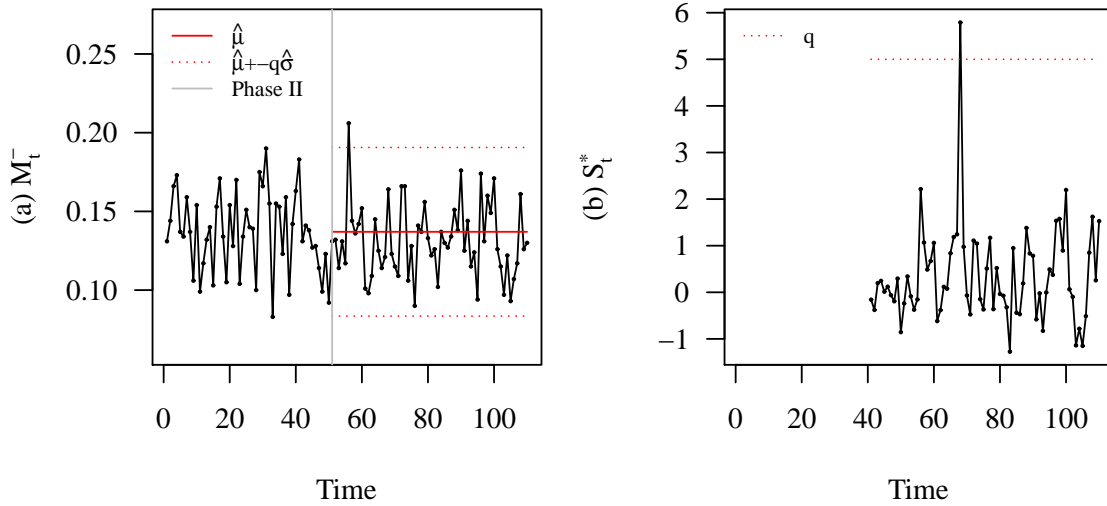


Figure 1: Illustration of General Monitoring Approaches for (a) M_t^- and (b) S_t^* . Plot (a) shows a Shewhart individuals control chart for M_t^- where control limits are calculated using Phase I data, and plot (b) shows a moving window approach on S_t^* using a pre-determined threshold. In this illustration, both methods signal around time-point 60.

2.2.1 Estimating Standard Deviation of Summary Statistics

To determine how to appropriately estimate the standard deviation of our summary statistics, we compare the standard \overline{MR}/d_2 , i.e., average moving range (AMR), with two alternatives. The first alternative is to use the median of the moving ranges, median moving range (MMR). The second alternative is using a correlated data calculation for standard deviation (SD), $s = \sqrt{\frac{s^2}{\gamma_1}}$ such that

$\gamma_1 = 1 - \frac{2}{(n-1)} \sum_{\kappa=1}^{n-1} \left(1 - \frac{\kappa}{n}\right) \rho_\kappa$ and ρ_κ is autocorrelation at lag κ (Box et al., 2008). These three measures of standard deviation are compared by the rate of false alarms above the upper control limit, $\hat{\mu} + q \cdot \hat{\sigma}$, where $\hat{\mu} = \bar{x}$, $q \in [2, 4]$, and $\hat{\sigma}$ is s for SD, \overline{MR}/d_2 for AMR, and median of MR values multiplied by 1.047 for MMR (Montgomery, 2007).

Results of 200 simulations were obtained using Phase I data with 100 nodes, $T_1 = 50$ time-periods for comparing metrics, and data generated from two common network models: the Dynamic Latent Space Model (DSLM) and the Dynamic Degree-Corrected Stochastic Block Model (DDCSBM). Details on models and model settings are described later in Section 3. Figure 2 shows four examples of false alarm rates with Figures 2 (a) and (b) from a DSLM count setting using $E[W_t]$ at 3% and at 18% respectively and with Figures 2 (c) and (d) from a DDCSBM count setting using ϕ at 0.10 and at 0.95. As seen in the figures, false alarm rates from control limits using SD and AMR perform similarly (solid and dashed lines in Figure 2), but MMR results in a larger number of false alarms when considering control limits between 2 to 4 standard deviations above the mean (dotted lines in Figure 2). Thus, to account for the correlation in monitoring dynamic network statistics and to obtain the smallest false alarm rates, the SD calculation is used as $\hat{\sigma}$ in calculating the control limits.

2.2.2 Determining Appropriate Thresholds

We ascertain if 3σ limits are appropriate in addition to suitable thresholds for monitoring the scan statistic, S_t^* . When monitoring the averages of batches via a Shewhart \bar{X} chart and conditioning on Phase I data, there are several approaches to determine appropriate control limits (Jardim et al., 2019). Similar principles from the \bar{X} chart can be used in our context for summary statistics. In general, we aim to fix the conditional false alarm probability for a statistic x_t such that $Pr(x_t > \hat{\mu} + q\hat{\sigma}) = p$. When monitoring the scan statistic, the method signals when the scan statistic is above a threshold (Priebe et al., 2005). The threshold recommended by Priebe et al. (2005) is 5, while in Zhao et al. (2018a) the authors showed via simulation study that perhaps lowering the threshold with a tolerable rate of false alarms can improve the performance of the scan statistic. For the scan statistic, we have the conditional false alarm probability as $Pr(x_t > q) = p$. Ultimately, p is determined by the practitioner, but in this work, we settle on $p = 0.03$. After calculating \bar{x} , using the correlated standard deviation s , and setting p , we must calibrate to obtain an appropriate q .

There are several ways to calibrate an appropriate q in thresholds of network monitoring. One option is if x_t reasonably follows a normal distribution (or some other well-known distribution), then q can be set using one-tail probabilities of the normal distribution, p . However, this method can lead to errors when the normality (or standard distribution) assumption fails to hold. Another option is empirically obtaining false alarm rates, the rate of signals for data with no anomalies. False alarm rates can be calculated from Phase I data or generated Phase II data with no anomalies. In practice, one does not know whether there is any anomaly in Phase II, and therefore only Phase I data should be used for calibrating q . However, there can be a difference between nominal false alarm rates (calibrated using Phase I data) and actual false alarm rates (resulting from Phase II data) in this approach. This happens due to sampling variation as the distribution of Phase II data, even when non-anomalous, is unlikely to be an exact replicate of Phase I data. In our case, we used synthetic network data for performance assessment. Since data are generated, Phase II data are generated from the same distribution as Phase I data. Therefore, established control limits

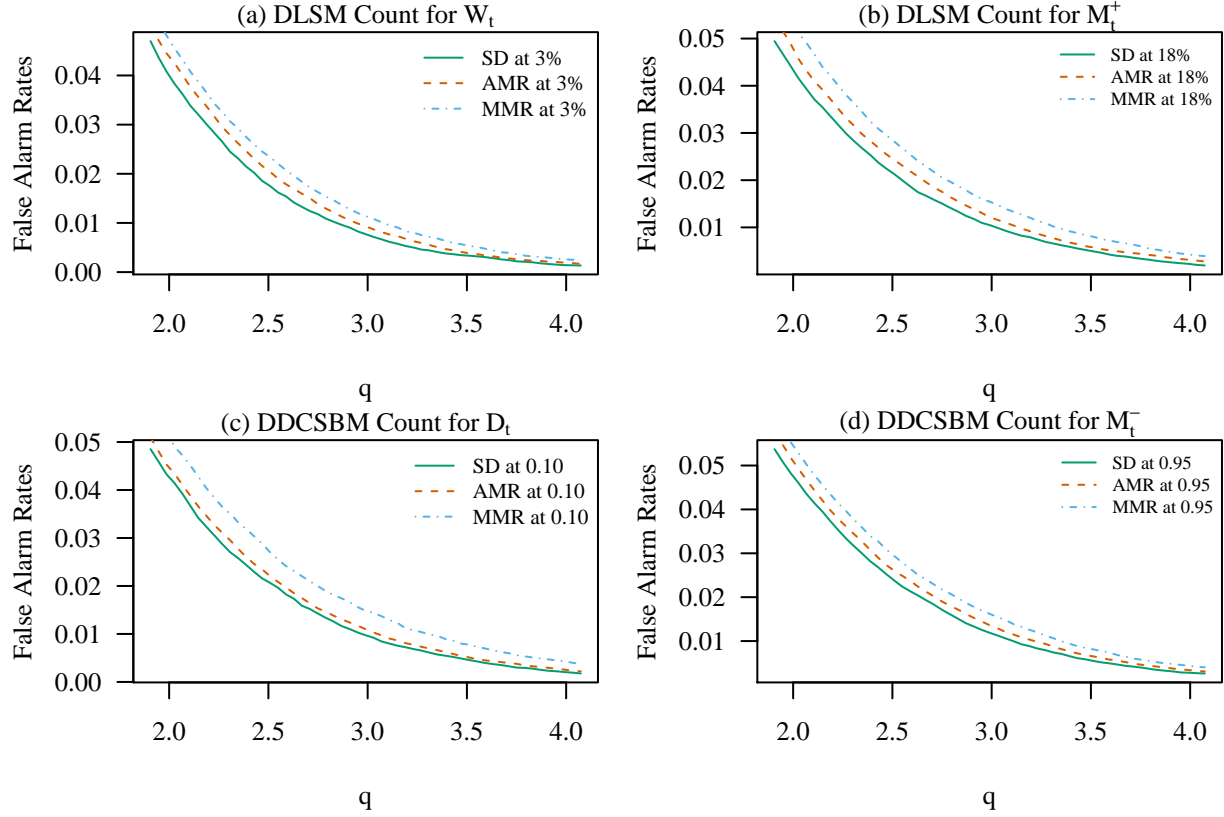


Figure 2: False Alarm Rates of AMR, MMR, and SD as $\hat{\sigma}$ in Control Limits, $\bar{x} + q \cdot \hat{\sigma}$, with $q \in [2, 4]$ across W_t , M_t^+ , D_t , and M_t^- . Plots (a) and (b) DLSM Count with Sparsity Levels and plots (c) and (d) DDCSBM Count with Correlation Levels. Dashed lines correspond to control limits using AMR, dotted lines are for MMR, and solid lines are for SD. False alarm rates are the lowest in all settings when using SD as $\hat{\sigma}$.

from Phase I data can be applied in Phase II data. This allows an exact calibration of false alarm rates in Phase II, which allows us to accurately compare the anomaly detection performance of the various summary statistics and the scan statistic of Priebe et al. (2005).

To determine if summary statistics approximately follow a normal distribution, empirical false alarm rates were compared to that based on the upper tail of a standard normal distribution, $Pr(Z > q)$. Here, false alarm rates are calculated using Phase II data with the same conditional false alarm probability as Phase I. Specifically in a Shewhart individuals control chart, the number of times x_t exceeds $\bar{x} + qs$ is recorded, and for the scan statistic, the number of times x_t exceeds q . Calibrating q is determined empirically using false alarm rates across varying correlation and sparsity values. Correlation is denoted using ϕ and sparsity is average density denoted using $E[W_t]$. Further details on models, model settings, and correlation and sparsity values are discussed in Sections 2 and 4. Monte Carlo simulations were performed a total of 1000 times using 100 nodes ($n = 100$) and 110 time-points ($T = 110$) in monitoring W_t , D_t , M_t^- , M_t^+ and S_t^* . For each simulation, all 110 time-points were simulated from the same model with Phase I data set at time-points up to time 50. Then, control limits are estimated from Phase I data, and the number of false alarms are calculated starting at time-point 51. To obtain false alarm rates, counts of false

alarms across 1000 simulations are summed together and divided by 1000. An example in binary DLSM and DDCSBM settings is shown for monitoring the scan statistic in Figure 3. As can be seen in Figure 3, false alarm rates are generally double or triple that of the area of the upper tail of a standard normal distribution for the scan statistic when varying the threshold of q between $[2, 4]$. False alarm rates tended to increase as correlation increases in the binary DLSM setting.

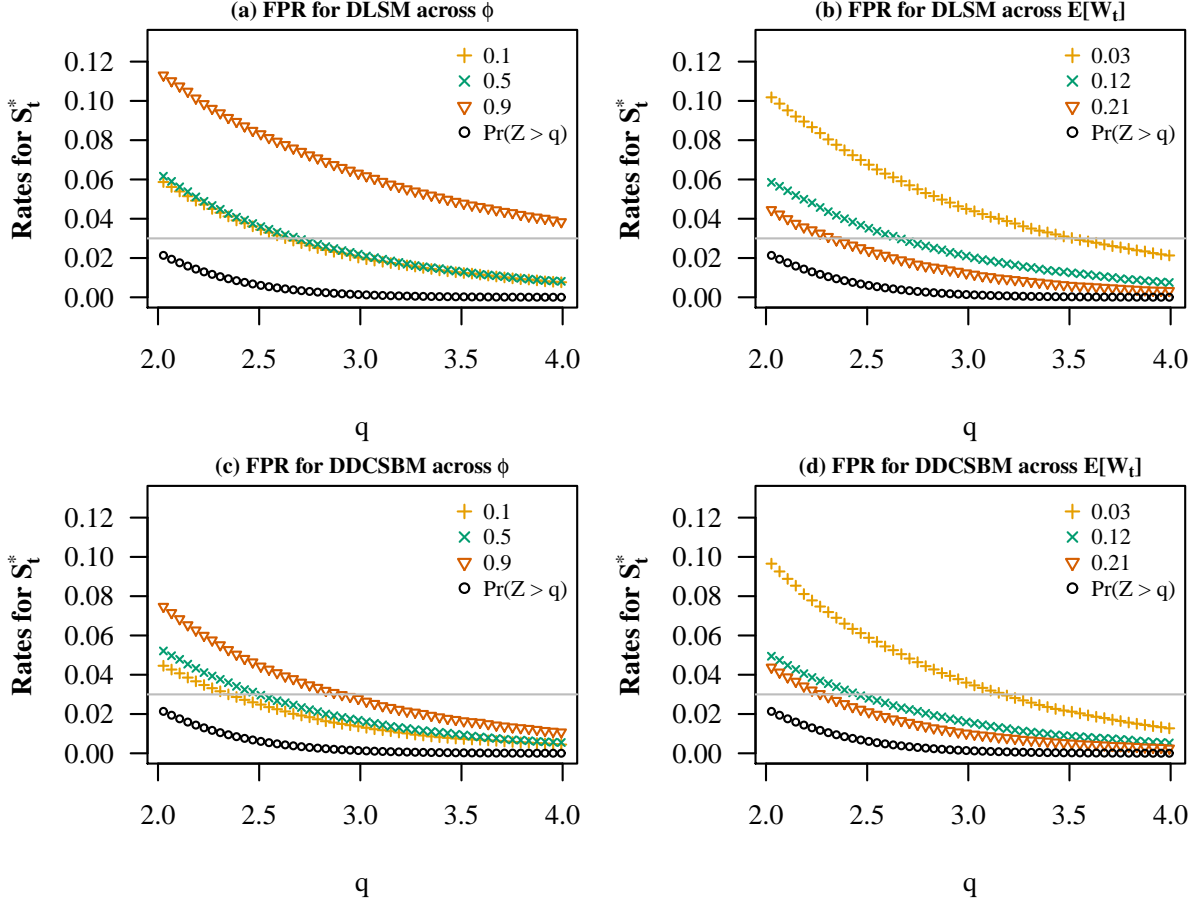


Figure 3: Plot of False Alarm Rates Monitoring S_t^* Across Varying Correlation [(a) and (c)] and Sparsity [(b) and (d)] in Binary DLSM and DDCSBM Settings.

Examples for binary or count networks are shown in Figures 10- 13 in Appendix A.1 for W_t , D_t , M_t^- , and M_t^+ . In general, there is less of a pattern between correlation and false alarm rates as well as sparsity and false alarm rates in the DDCSBM setting. In the DLSM setting, higher correlation tends to increase false alarm rates when monitoring with these methods, while varying correlation and sparsity has little effect in the DDCSBM setting. Hence, $p = 0.03$ is used as our false alarm threshold to accommodate those statistics which do not follow a normal distribution and have higher false alarm rates than that obtained using the upper one-sided tail of a standard normal distribution. Then, q is calibrated from empirical false alarm rates as close as possible to $p = 0.03$.

3 Statistical Models for Dynamic Networks

Our methods for anomaly detection do not rely on a parametric model. Therefore, we neither have to estimate parameters of such a model nor determine if parameter estimates had changed significantly. Rather, we use statistical models to generate synthetic network data, and then implement the model-free methods on these synthetic networks. We highlight this advantage of a model-free approach to parametric based methods by generating dynamic network data from two popular latent variable models. Kim et al. (2018) reviewed several latent variable models including latent space models and stochastic block models in both static and dynamic versions. Specifically, we focus on particular formulations of a dynamic latent space model (DLSM) and dynamic degree-corrected stochastic block models (DDCSBM).

3.1 Dynamic Latent Space Model

Use of latent space models relies on defining a space of latent positions using either pairwise distances or projections (Kim et al., 2018). Hoff et al. (2002) introduced both a distance based and projection based latent space model using Bayesian inference for parameter estimation via MCMC. The idea here is that the probability of forming an edge between nodes i and j depends on the latent positions z_i and z_j . For example, z_i and z_j being relatively close together (via a distance metric) in the latent space suggests a higher probability of an edge between nodes i and j in the network. Hence, edges are conditionally independent given the latent positions. We focus on the formulation of Sewell and Chen (2015) who extended ideas of Hoff et al. (2002) to a dynamic version of a latent space model.

We now provide an overview of the DLSM in Sewell and Chen (2015). More details can be found in their paper. Let \mathbf{Y}_t be an adjacency matrix at time $t \in \{1, 2, \dots, T\}$ such that $y_{ijt} = 1$ when there is an edge between nodes i and j and 0 otherwise. Let \mathbf{X}_t be a matrix of latent positions ($\mathbf{X}_{it} = (x_{it1}, x_{it2})$ for node $i \in \{1, 2, \dots, n\}$) at time t . For ease in plotting and visualizations, two-dimensional coordinates are used. The probability of an edge between nodes i and j is given by

$$y_{ijt} \mid \Psi = \{\mathbf{X}_{it}, \mathbf{X}_{jt}, \beta_{IN}, \beta_{OUT}, \mathbf{r}, \sigma^2\} \sim \text{Bern} \left(p_{ijt} = \frac{\exp(\eta_{ijt})}{1 + \exp(\eta_{ijt})} \right) \text{ s.t.}$$

$$\eta_{ijt} = \log \left(\frac{\Pr(y_{ijt} = 1 \mid \Psi)}{\Pr(y_{ijt} = 0 \mid \Psi)} \right) = \beta_{IN} \left(1 - \frac{d_{ijt}}{r_j} \right) + \beta_{OUT} \left(1 - \frac{d_{ijt}}{r_i} \right).$$

The parameters β_{IN} and β_{OUT} are global (system-scale) network characteristics describing popularity and social activity respectively. If $\beta_{IN} > \beta_{OUT}$ in a directed network, then this suggests the receiver is more important while the opposite scenario suggests the sender is more important. The radii in $\mathbf{r} = (r_1, r_2, \dots, r_n)$, are node specific characteristic describing the radius of communication in the latent space such that the radii sum to 1, i.e., $\sum_{i=1}^n r_i = 1$. These radii are analogous to a scaled degree of a node. The pairwise distance between latent positions of nodes i and j is denoted as $d_{ijt} = \text{dist}(\mathbf{X}_{it}, \mathbf{X}_{jt})$, and the spread of the latent positions are controlled by σ^2 .

In order to generate data from this model, we use the prior distribution on latent positions to get $\mathbf{X}_{1:T}$ and subsequently d_{ijt} and set values for the remaining parameters, β_{IN} , β_{OUT} , \mathbf{r} , and σ^2 . The original prior in Sewell and Chen (2015) is $N(\mathbf{0}^T, \tau^2 I_2)$ for the initial network and $N(\mathbf{X}_{i(t-1)}, \sigma^2 I_2)$ for all subsequent networks. Hence, a priori, latent positions may move around the space according

to some random jump (dictated by τ^2 or σ^2). For meaningful networks, the variances of the latent positions must be quite small in order to achieve reasonable edge probabilities. We demonstrate how latent positions move a priori in Figure 4 using $T = 100$, $\sigma^2 = 0.0003$ and 5 clusters (defined by both color and shape). Latent positions are plotted at times $t = 2, 36, 58$, and 100 in plots (a)-(d) respectively. As time increases, we observe a spread of latent positions from the initial tight clusters. Perhaps intermixing of clusters is desired a priori, but the spread of latent positions has an effect on edge probabilities, p_{ijt} . By increasing pairwise distances of the latent positions, d_{ijt} , this decreases p_{ijt} values over time, and in turn, decreases realizations of p_{ijt} values via network density. An interpretation of Figure 4 is that people communicate less and less as over time, which may not make practical sense. Thus, generating latent positions from this distribution is a concern due to the spread in latent positions.

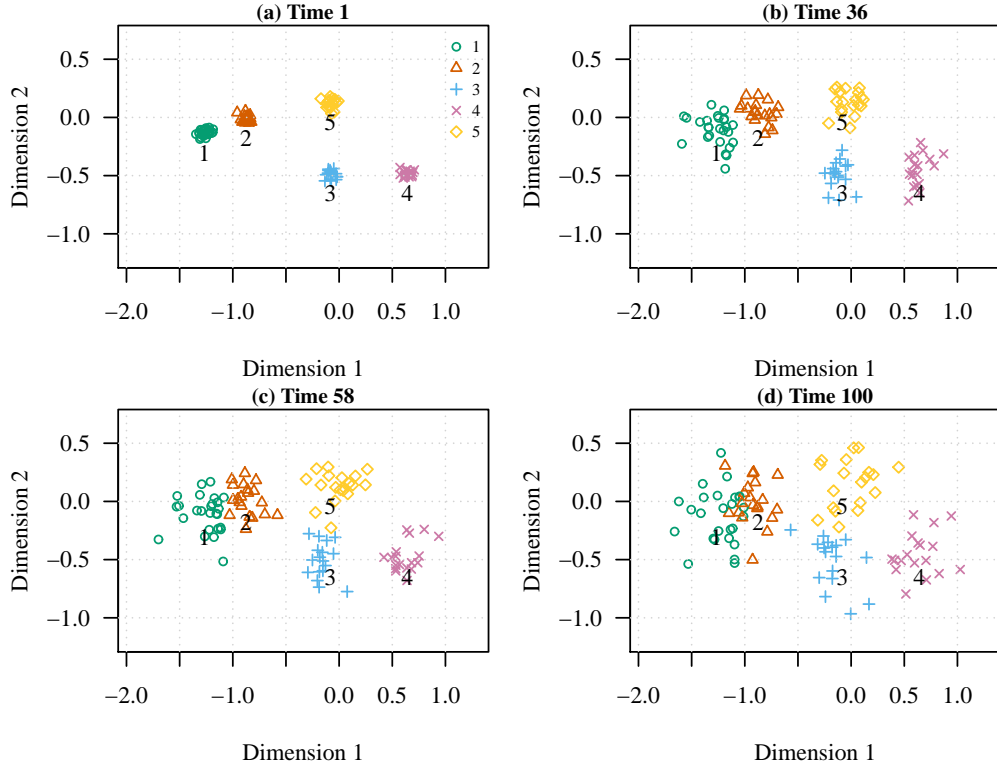


Figure 4: Latent Positions at Times (a) 2, (b) 26, (c) 58, and (d) 100. For $\sigma^2 = 0.0003$ and $T = 100$, the spread of the latent positions grow over time when starting in tight pre-defined clusters.

Our solution is to scale the spread of the latent positions, σ^2 , using a time series model, in particular, a vector auto-regression of order 1 (VAR(1)) model. Consider the following VAR(1) model:

$$\mathbf{X}_{i(t+1)} = \phi \cdot \mathbf{X}_{it} + \boldsymbol{\epsilon}_{t+1} \Rightarrow \begin{bmatrix} x_{i1(t+1)} \\ x_{i2(t+1)} \end{bmatrix} = \phi * \begin{bmatrix} x_{i1t} \\ x_{i2t} \end{bmatrix} + \begin{bmatrix} \epsilon_{1(t+1)} \\ \epsilon_{2(t+1)} \end{bmatrix},$$

such that $|\phi| < 1$ and $\boldsymbol{\epsilon}_{t+1} \sim N((0,0)^T, \sigma^2 I_2)$. Thus, a VAR(1) prior on latent positions has the

following form:

$$\begin{aligned}\mathbf{x}_1 \mid \phi, \sigma^2 &\sim \prod_{i=1}^n N\left(\mathbf{0}, \tau^2 = \left(\frac{\sigma^2}{(1-\phi^2)}\right) I_2\right) \\ \mathbf{x}_t \mid \mathbf{x}_{t-1}, \phi, \sigma^2 &\sim \prod_{i=1}^n N\left(\mathbf{x}_{i(t-1)}, \tau^2 = \frac{\sigma^2}{(1-\phi^2)} I_2\right), \text{ for } t \geq 2.\end{aligned}$$

We compare the network densities from the original prior to a VAR(1) prior when $n = 100$, $T = 100$, $\beta_{IN} = \beta_{OUT} = 1$, $\mathbf{r} = \{1/n\}$, $\phi = 0.3$, and $\sigma^2 = 0.0003$ in Figure 5. Network density is plotted over time, and we observe a decay in density using the original prior whereas density using a VAR(1) prior is within a reasonable range around an average density of 11%. Thus, using a VAR(1) prior appears able to control the spread of the latent positions a priori over time.

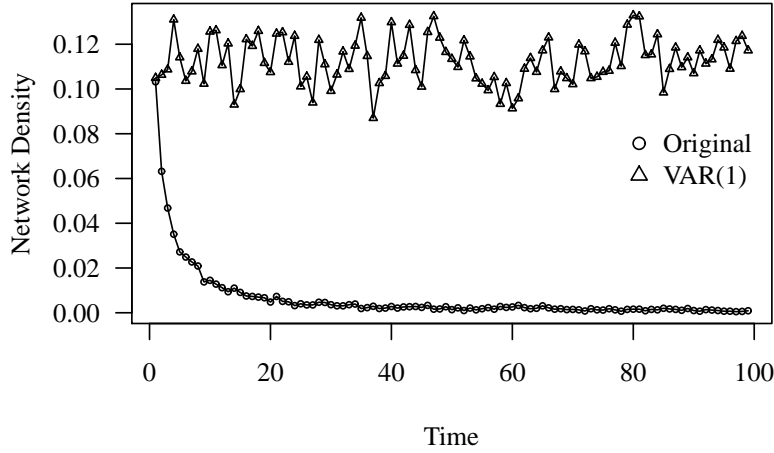


Figure 5: Network Density using Original Prior and VAR(1) Prior on Latent Positions with $n = 100$, $T = 100$, $\beta_{IN} = \beta_{OUT} = 1$, $\mathbf{r} = \{1/n\}$, $\phi = 0.3$, and $\sigma^2 = 0.0003$.

By default, the model is setup as a binary network, but we can make the following modification for a count network: $y_{ijt} \mid \Psi \sim \text{Poisson}(p_{ijt} = \exp\{\eta_{ijt}\})$ s.t. $\eta_{ijt} = \log(E[y_{ijt} \mid \Psi])$ (Sewell and Chen, 2016). Default settings of parameters in the simulation study include $\sigma^2 = (1 - \phi^2)$, $\beta_{IN} = 1$, $\beta_{OUT} = 2$, and $\mathbf{r} = \{\frac{1}{n}\}_{i=1}^n$. An outline of the data generation from a DLSPM is provided in Algorithm 3.

3.2 Dynamic degree-corrected stochastic block model

Stochastic block models (SBM), on the other hand, utilize a latent community (block) assignment to assign edge probabilities (Snijders and Nowicki, 1997). That is, edge probabilities within a community should differ from edge probabilities between communities. Matias and Miele (2017) extended an SBM model to a dynamic version which highlights evolving community memberships over time as well as any desired probability density measure on edge probabilities. A general issue with SBMs is when degree is heterogeneous among nodes (Karrer and Newman, 2011). Many times, communities of high degree nodes and low degree nodes are formed, which may not be

Algorithm 3 Data Generation from a DLSM.

- 1: Set $n, T, \phi, \sigma^2, \beta_{IN}, \beta_{OUT}, \mathbf{r}$ and choose binary or count network.
 - 2: Generate latent positions, $\mathbf{X}_{1:T}$, using ϕ and σ^2 .
 - Set number of clusters and draw means for each cluster using $N(\mathbf{0}, (2/n)^2 I_2)$.
 - Assign cluster labels to n nodes.
 - Generate \mathbf{X}_1 by drawing from a normal distribution with assigned cluster mean and variance $\sigma^2 I$.
 - Generate $\mathbf{X}_{2:T}$ using $\mathbf{X}_t = \phi \cdot \mathbf{X}_{t-1} + N(0, \sigma^2)$. *Note: For stationarity, generate an additional T latent positions and keep last T draws.*
 - 3: Calculate pairwise distances of latent positions.
 - 4: **For** t **in** $1 : T$ **{**
 - For** i **in** $1 : n$ **{**
 - Get $\eta_{ijt} = \beta_{IN} \left(1 - \frac{d_{ijt}}{r_j}\right) + \beta_{OUT} \left(1 - \frac{d_{ijt}}{r_i}\right)$.
 - Draw $y_{ijt} \sim \text{Bern}\left(p_{ijt} = \frac{\exp(\eta_{ijt})}{1 + \exp(\eta_{ijt})}\right)$ (binary) or $y_{ijt} \sim \text{Poisson}(p_{ijt} = \exp\{\eta_{ijt}\})$ (count) .
 - }** **END**
 - }** **END**
-

appropriate community assignments. Karrer and Newman (2011) developed a degree-corrected version of an SBM (DCSBM). Wilson et al. (2019) discussed a dynamic version of a DCSBM utilizing parameters to describe a propensity for a node to communicate. The DDCSBM model we use to generate data from adapts the dynamic SBM of Matias and Miele (2017) to include degree heterogeneity and the dynamic DCSBM of Wilson et al. (2019) to include correlation over time in the propensities. Ultimately, we use a model that allows for movement within community assignment, degree heterogeneity, and correlation among propensities to communicate over time.

We now provide an overview of the adapted DDCSBM used for data generation. Let \mathbf{Y}_t represent an adjacency matrix at time t for $t \in \{1, 2, \dots, T\}$. Let K represent the number of communities and the probability of an edge between nodes i and j is defined by:

$$y_{ijt} \sim \text{Poisson}(p_{ijt} = \theta_{it}\theta_{jt}\omega_{Z_{it}Z_{jt}}).$$

Parameter Z_{it} is a latent community assignment for node i at time t . The initial assignment is found via $Z_{i0} \sim \text{Multinomial}(\boldsymbol{\alpha} = \{1/K\}_{k=1}^K)$, and for all subsequent networks, community assignments can transition with probability $\boldsymbol{\pi}_{K \times K}$, where

$$\boldsymbol{\pi}_{K \times K} = \begin{pmatrix} \boldsymbol{\pi}_1 \\ \boldsymbol{\pi}_2 \\ \vdots \\ \boldsymbol{\pi}_K \end{pmatrix} = \begin{pmatrix} \pi_{11} & \pi_{1K} & \cdots & \pi_{1n} \\ \pi_{21} & \pi_{22} & \cdots & \pi_{2K} \\ \vdots & \vdots & \ddots & \vdots \\ \pi_{K1} & \pi_{K2} & \cdots & \pi_{KK} \end{pmatrix}$$

such that if $Z_{it} = k$, $Z_{i(t+1)} \sim \text{Multinomial}(\boldsymbol{\pi}_k)$ for $k \in \{1, 2, \dots, K\}$. Next, we introduce propensity to communicate parameters, $\boldsymbol{\Theta} = \{\boldsymbol{\theta}_1, \boldsymbol{\theta}_2, \dots, \boldsymbol{\theta}_n\}$ such that $\boldsymbol{\theta}_i = \{\theta_{i1}, \theta_{i2}, \dots, \theta_{iT}\}$

and $\theta_{it} \in [1 - \delta, 1 + \delta]$ for some $\delta \in (0, 1)$ (Wilson et al., 2019). A low propensity to communicate suggests the degree of that node will be relatively low. Parameter $\omega_{K \times K}$ is community structure matrix such that $\omega_{Z_{it}Z_{jt}} \in (0, 1)$ and $\text{diag}(\omega)$ are all distinct values. As noted in Matias and Miele (2017), if any intra-community communication values are the same, then distinguishing those communities remains unidentifiable. Community assignments affect propensities in the following way. Propensities of communication for a given community must be rescaled by the average propensity to preserve community structure. That is, if nodes transition between communities, then corresponding θ_{it} will be rescaled as will the average propensity for those communities at time t .

We specify the following “white noise” process to incorporate correlation. First, $\theta_{i0}^* \sim U(-1, 1)$ for all nodes i . Next,

$$\theta_{it}^* = \phi \cdot \theta_{i0}^* + (1 - \phi) \cdot \epsilon_{it} \text{ such that } \epsilon_{it} \sim U(-1, 1) \text{ and } |\phi| < 1. \quad (6)$$

Then, $\theta_{it} = \delta * \theta_{it}^* + 1$ so that $\theta_{it} \in [1 - \delta, 1 + \delta]$ for some $\delta \in (0, 1)$. In Equation 6, ϵ_t is scaled in order to achieve $\theta_{it} \in [1 - \delta, 1 + \delta]$. The reason for using a constant $\phi \cdot \theta_{i0}^*$ in Equation 6 rather than a more traditional AR(1), i.e., $\phi \cdot \theta_{i(t-1)}^*$, is that we want propensities to stay within a reasonable range of their starting value as $|\phi| \rightarrow 1$. After transformation when using an AR(1) model, we have the mean of the series as 1 with variance of $(1 - \phi)^2 \sigma_\epsilon^2 / (1 - \phi^2)$. An issue is regardless of the starting value of a propensity, the AR(1) process tends toward the mean of 1 (after transformation). This implies, if $\theta_{i0}^* = -0.75$ and $\delta = 0.98$ so that $\theta_{i0} = \delta \cdot \theta_{i0}^* + 1 = 0.265$, then an AR(1) process with $\phi = 0.90$ for θ_i settles around 1 rather than around $\theta_{i0} = 0.265$. We illustrate this tendency toward the mean of the process in Figure 6 using $\theta_{i0} = 0.265$ (shown using an asterisk) and $\delta = 0.98$ at a relatively low and high correlation, $\phi = 0.30, 0.90$. In Figure 6, we contrast an AR(1) model with our “white noise” model given in Equation 6 using the same ϵ values for both processes. Thus, low or high propensity to communicate nodes would be washed out if using a traditional AR(1) model. Therefore, scaling a “white noise” type process introduces a different kind of correlation based on the initial starting value of a propensity as can be seen in Figure 6.

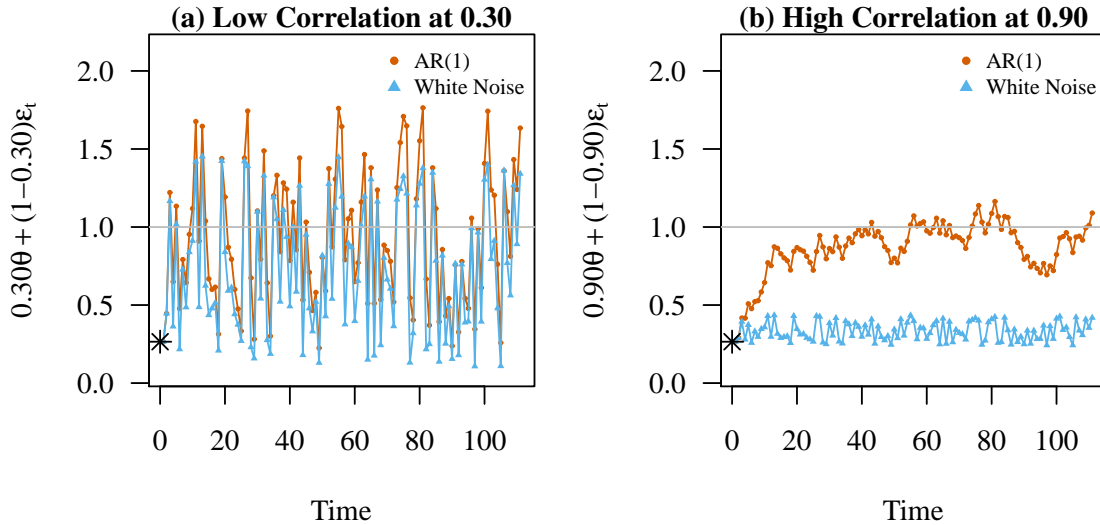


Figure 6: AR(1) Model and White Noise at $\phi = 0.30$ (a) and 0.90 (b) for θ using $\delta = 0.98$ and $\theta_0 = 0.265$.

The default edge type is counts for the DDCSBM, but for any threshold, $b \in \mathbb{N}$, we can turn edge counts into a binary network. In this work, we use $b = 1$ to obtain a binary network such that $y_{ijt}^* = 1$ if $y_{ijt} \geq b$. Settings of parameters in the simulation study include $K = 3$, $\delta = 0.98$,

$$\boldsymbol{\pi} = \begin{pmatrix} 0.96 & 0.02 & 0.02 \\ 0.02 & 0.96 & 0.02 \\ 0.02 & 0.02 & 0.96 \end{pmatrix}, \text{ and } \boldsymbol{\omega} = \begin{pmatrix} 0.7 & 0.2 & 0.25 \\ 0.2 & 0.6 & 0.3 \\ 0.25 & 0.3 & 0.5 \end{pmatrix}.$$

Three communities are chosen rather than two for some additional variation. The $\theta_{it} \in [0.02, 1.98]$ are re-scaled within each community by the average propensity of each community respectively. Relatively low transition rates to other communities are selected for $\boldsymbol{\pi}$. Lastly, intra-communication was chosen to be much higher than inter-communications to help identify communities (Matias and Miele, 2017). An outline of the data generation from a DDCSBM is provided in Algorithm 4. Lastly, notation used to generate data from dynamic networks is summarized in Table 2.

Algorithm 4 Data Generation from a DDCSBM.

- 1: Set $n, T, K, \phi, \delta, \omega$, and $\boldsymbol{\pi}$, and choose a binary or count network.
 - 2: Generate latent community assignments using K and $\boldsymbol{\pi}$.
 - Sample initial latent community assignments, $Z_{i0} \sim \text{Multinomial}(\boldsymbol{\alpha} = \{1/K\}_{k=1}^K)$.
 - Generate $Z_{it} \sim \text{Multinomial}(\boldsymbol{\pi}_k)$ for $Z_{i(t-1)} = k$.
 - 3: Generate propensities to communicate, $\boldsymbol{\Theta}$, using ϕ and δ .
 - Generate initial values $\{\theta_{01}^*, \theta_{02}^*, \dots, \theta_{0n}^*\} \sim U(-1, 1)$.
 - Generate $\boldsymbol{\theta}_i^*$ using $\theta_{it}^* = \phi \cdot \theta_{i0}^* + (1 - \phi) \cdot U(-1, 1)$.
 - Recalculate $\boldsymbol{\theta}_i = \delta * \boldsymbol{\theta}_i^* + 1$ for all nodes i .
 - 4: **For** t **in** $1 : T$ **{**
 - For** i **in** $1 : n$ **{**
 - Scale θ_{it} by the mean of propensities in community k : $\theta_{it}^* = \theta_{it} / \sum_{|k|} \theta_{jt}$.
 - Draw $y_{ijt} \sim \text{Poisson}(p_{ijt} = \theta_{it}\theta_{jt}\omega_{Z_{it}Z_{jt}})$ (count) or $y_{ijt}^* = \begin{cases} 0 & y_{ijt} = 0 \\ 1 & y_{ijt} \geq 1 \end{cases}$ (binary).
 - }** **END**
 - }** **END**
-

Symbol	Meaning
K	Number of communities (blocks)
β_{IN}	Global DLSM parameter for popularity
β_{OUT}	Global DLSM parameter for social activity
\mathbf{r}	DLSM parameter for radius of communication of all nodes
r_i	Radius of communication of node i
\mathcal{X}_t	Latent positions at time t in a DLSM
σ^2	DLSM parameter controlling spread of latent positions, $\mathcal{X}_{1:T}$
ϕ	correlation via a time series
π	DDCSBM parameter for community transition rate
Θ	DDCSBM parameter for propensity of communication for all nodes
θ_{it}	Propensity of communication for node i at time t
ω	Community structure matrix in a DDCSBM

Table 2: List of Notation Related to Data Generated from Dynamic Models.

4 Performance Evaluation of Monitoring Methods

Based on data generated from models explained in Section 3, we conducted a comprehensive simulation study to evaluate the performance of monitoring network density, maximum degree, linear combinations of maximum degree and network density, as well as the scan statistic. A simulation study may allow for better understanding and evaluation of network monitoring approaches and types of changes detectable in dynamic network data. Performance evaluation is accomplished as follows. First, temporally-evolving network data are generated according to simulation study settings discussed in 4.1. Second, general network monitoring approaches are applied to such network data as was discussed in Section 2.2. Last, metrics for evaluating network monitoring output is elaborated on in Section 4.2. To help facilitate understanding of performance evaluation output, effects of varying correlation and sparsity levels are briefly discussed in Section 4.3.

In our simulation study, we considered two types of anomalies: anomalies in edge probabilities and expected degree. All Monte Carlo simulations were performed using 100 nodes ($n = 100$) and 110 time-points ($T = 110$). For each type of anomaly, simulations were performed 200 times. Out of the 110 time-points, we set $T_1 = 50$, the first 50 time-points, as Phase I data where no anomalies are embedded. The latter 60 time-points ($t > 51$) are used as Phase II data with embedded anomalies in edge probabilities or expected degree for some duration. Performance evaluation from each type of anomaly is discussed respectively in Sections 4.4 and 4.5.

4.1 Simulation Study Settings

To evaluate performance of the methods based on summary statistics, temporally-evolving network data were simulated. Such simulated data take into account various amounts of correlation, sparsity, duration of anomaly, model, model parameters, and network types. Correlation is controlled by varying values of the VAR or white noise coefficient, ϕ , and sparsity is controlled by varying values of average density, $E[W_t]$. In particular, the values considered are

$$\phi \in \{0.1, 0.3, 0.5, 0.75, 0.9, 0.95, 0.99\} \text{ and } E[W_t] \in \{0.03, 0.06, 0.09, 0.12, 0.15, 0.18, 0.21\}.$$

Average density is fixed at 11%, $E[W_t] = 0.11$, when varying ϕ in order to mimic realistic network densities of application data. Likewise, ϕ is fixed at 0.5 when varying $E[W_t]$ so that correlation across time is not too high nor too low. Duration of anomaly or change point length (CPL) represents consecutive time periods in which some kind of anomaly occurs, typically ranging from 5 time-points to 25 time-points throughout the study. Both binary and count network types are considered in DLSD and DDCSBM settings.

In all our scenarios, negative correlation, e.g., $\phi = -0.5$, is not included. When exploring negative correlation in the context of dynamic networks, we found similar results with summary statistics on data generated using positive correlation. While performance is similar, the interpretation of such networks differs. In general, rather than nodes moving closer together or increasing the chance of a connection (form an edge), under negative correlation nodes may move farther apart or experience a decrease in the chance of a connection. For many brain studies and resulting dynamic networks applied on brain activity, correlation plays a big role in relating a behavior and the type of connections formed in the network (Hidalgo et al., 2009; Zabelina and Andrews-Hanna, 2016). In both application data examples of Hidalgo et al. (2009) and Zabelina and Andrews-Hanna (2016) on brain activity, negatively correlated activities in the brain tend to decrease the prevalence of a behavior or task.

For all simulations, we used the model settings described at the end of Sections 3.1 and 3.2. However, in order to achieve desired average densities, we must scale parameter(s) in network models using a scalar, a_ℓ . A subscript ℓ is used to distinguish between a binary ($\ell = 1$) and count ($\ell = 2$) network. We chose to scale parameters σ^2 in a DLSD and ω in a DDCSBM. Specific settings for $a_\ell \sigma^2$ in a DLSD and $a_\ell \omega$ in DDCSBM are provided for ease of replicating results in our simulation study. When varying ϕ and controlling average network density at around 11%, in a DLSD, $a_1 = 0.00014$ and $a_2 = 0.00042$ for $a_\ell \sigma^2$, and in a DDCSBM, $a_1 = 0.16$ and $a_2 = 0.17$ for $a_\ell \cdot \omega$. When varying $E[W_t]$ and fixing $\phi = 0.5$, specific settings of a_ℓ to appropriately scale σ^2 and ω are given in Table 3.

Model	a_ℓ	Average Network Density $E[W_t]$						
		0.21	0.18	0.15	0.12	0.09	0.06	0.03
DLSD	a_1	0.0002	0.0002387	0.000292	0.000373	0.000493	0.000747	0.00153
	a_2	$3.5 \cdot a_1$	$3.4 \cdot a_1$	$3.4 \cdot a_1$	$3.3 \cdot a_1$	$3.3 \cdot a_1$	$3.3 \cdot a_1$	$3.3 \cdot a_1$
DDCSBM	a_1	0.35	0.29	0.24	0.18	0.14	0.09	0.045
	a_2	0.32	0.265	0.22	0.17	0.13	0.085	0.045

Table 3: Scalar Settings of $a_\ell \sigma^2$ and $a_\ell \omega$ for Binary ($\ell = 1$) and Count ($\ell = 2$) Networks when Varying $E[W_t]$.

4.2 Performance Evaluation Metrics

Using the settings described in Section 4.1, network data were generated and network monitoring approaches were applied as discussed in Section 2.2. For each Monte Carlo simulation, the output of network monitoring approaches is a binary stream output, \mathbf{A} , where $A_t = 1$ if the method signals, and $A_t = 0$ otherwise. Performance evaluation of output from network monitoring approaches is accomplished using two measures. One such measure is detection rate (DR), which is a binary

measure of whether or not an anomaly was detected at all. If an anomaly is detected that outcome is assigned a 1 and 0 otherwise. DR provides a measure of the ability of a network monitoring approach to find anomalies. To further quantify this ability, a second measure utilized is AUC calculations from ROCs. In this context, we take advantage of confusion matrices. True labels of a confusion matrix are the time periods (t) within the duration of an anomaly, and predicted labels are alarms found from signals of network monitoring approaches. In a resulting ROC curve, both the true positive rate (TPR) and false positive rate (FPR) must range from $[0,1]$. Thus, we vary q from -6 to 6, i.e., $q \in [-6,6]$, in control limits $CL = \hat{\mu} + q\hat{\sigma}$ and threshold q for the scan statistic to achieve desired FPR and TPR in $[0,1]$. In essence, AUC reflects the number of times an anomaly is detectable. Both DR and AUC are calculated in each Monte Carlo simulation and later averaged over all Monte Carlo simulations.

4.3 Effects of Correlation and Sparsity on Summary Statistics

We explore the effect of correlation (ϕ) and sparsity ($E[W_t]$) on means and standard deviations of summary statistics in Phase I data. Recall when monitoring summary statistics, control limits of a Shewhart individuals control chart are $\bar{x} \pm qs$. Choosing an appropriate q was discussed in Section 2.2.2, but learning the effects of correlation and sparsity on \bar{x} and s can aid understanding of the evaluation of network monitoring. Phase I data correspond to time-points less than 50, $t \leq 50$. Figures 14-21 are provided in Appendix A.2 displaying means and standard deviations of W_t , D_t , M_t^- , and M_t^+ across varying amounts of correlation and sparsity. Examples across varying correlation, i.e., ϕ , are shown for a binary DLSP and count DDCSBM settings and across varying sparsity, i.e., $E[W_t]$, are shown for count DLSP and binary DDCSBM. In DLSP settings, as correlation increases, the range of the means widens. In DDCSBM settings, this mainly affects means of maximum degree and subsequently the sum and difference statistics. The standard deviation is less affected by correlation overall. In terms of varying sparsity, actual values of the means vary while both range and values of the standard deviation change in DLSP and DDCSBM settings. In summary, the means more so than standard deviations of W_t , D_t , M_t^- , and M_t^+ are affected by correlation and sparsity.

4.4 Performance Evaluation with Anomalies in Edge Probabilities

We design a set of simulations to ultimately affect network density by manipulating p_{ijt} (edge probabilities) in simulated network data. Such manipulation is accomplished via an odds ratio, denoted OR . For a DLSP, $y_{ijt} \sim \text{Bern}(p_{ijt})$. Hence, for a given OR , we compare $p_0 = p_{ijt}$ and $p_1 = C_{ijt} \cdot p_{ijt}$ such that $OR = \left(\frac{1-p_0}{p_0}\right) / \left(\frac{1-p_1}{p_1}\right)$ and $C_{ijt} = \frac{OR}{(1-p_0+OR \cdot p_0)}$. Thus, as OR increases, so does C_{ijt} . For a DDCSBM, $y_{ijt} \sim \text{Pois}(p_{ijt})$. Since p_{ijt} is a rate, we directly compare p_{ijt} and $OR \cdot p_{ijt}$. Such an anomaly implies a group of nodes all of a sudden increase (or decrease) communication. Specific scenarios are described in Table 4. Shift size refers to a medium or large change in resulting density. Let N denote the number of nodes affected by a given change.

Shift Size	Network Type	Number of Anomalous Nodes (N)	OR Change from 1 to
Medium	DLSM	33	4
Medium	DDCSBM	33	2.5
Large	DLSM	79	2.5
Large	DDCSBM	72	1.5

Table 4: Scenarios for Simulation Study Targeting Network Density via Odds Ratio.

An example using $N = 33$ anomalous nodes and OR change from 1 to 4 is shown in a binary DLSM and DDCSBM in Figure 7 with $\phi = 0.5$, $E[W_t] = 0.11$, and settings mentioned in Section 4.1. Shewhart control charts for this example are plotted for M_t^- and M_t^+ with Phase I data for $t \leq 50$ in Figure 7. The solid red line indicates the mean from Phase I, the dashed red lines indicate q standard deviations above or below the mean, the gray line separates Phase I and Phase II, and the blue dashed lines indicate the beginning and ending of the CPL. The number of standard deviations above the mean was determined by controlling the false alarm rates in the non-anomalous empirical data for $p = 0.03$ and $\phi = 0.5$ as was discussed in Section 2.2.2.

It is difficult to find meaningful changes to lower the odds ratio in the DLSM setting since manipulating p_{ijt} (edge probabilities) closer to 0 appears to be affected by the randomness of latent positions. That is, the closer two latent positions are, the higher the edge probability becomes. It could be the case that two latent positions are so close together, that even scaling such edge probability yields a $p_{ijt} > 0.2$. Thus, only scenarios increasing the odds ratio are considered.

Results of 200 simulations with $n = 100$, $T = 110$, and $CPL = 5, 10$, or 15 are summarized below in Tables 5 -8 using DR and in Appendix A.3 Tables 18 -21 using AUC. The values corresponding to the method which detects the planted anomaly best are in bold. Since anomalies planted affect edge probabilities (and ultimately density), it would be natural for the monitoring using W_t to detect this change the best. Results are explained first by model and network type settings and then across trends in CPL, correlation, and sparsity. In binary DLSM settings, the best monitoring performance in terms of detection rates in the medium shift size case vary between D_t , M_t^- , and M_t^+ , while W_t performs best in the large shift size case.

In nearly all count DLSM settings, monitoring W_t , D_t , M_t^- , and M_t^+ all detect perfectly with a DR of 1. The worst performer tends to be S_t^* in DLSM settings, but the DR of the scan statistic method is high in count DLSM settings with a large shift size. In DDCSBM settings, the best performer is almost always W_t , which we would expect since the anomaly affected edge probabilities. In count DDCSBM settings, M_t^+ method does best, and in the large shift size setting, S_t^* method also has a perfect detection rate. The shorter the duration, higher the correlation, and higher in sparsity, the worse most methods do in detecting an anomaly. These trends are observed more so in binary DLSM settings. From count to binary DDCSBM settings, recall that count data are transformed into binary using $y_{ijt}^* = 1$ if $y_{ijt} \geq 1$. In some cases, performance is better in count settings, but not in others.

We make note the design of S^* method is to detect if a change occurred rather than to identify the time-points said change occurred in (Priebe et al., 2005; Zhao et al., 2018a). That is, when monitoring the scan statistic, the method is expected to signal at best only a few times if any anomaly occurred. In AUC results reported in Tables 18 -21 in Appendix A.3, the detection ability is mainly best for M_t^- and M_t^+ methods in DLSM settings while the W_t method does detect best

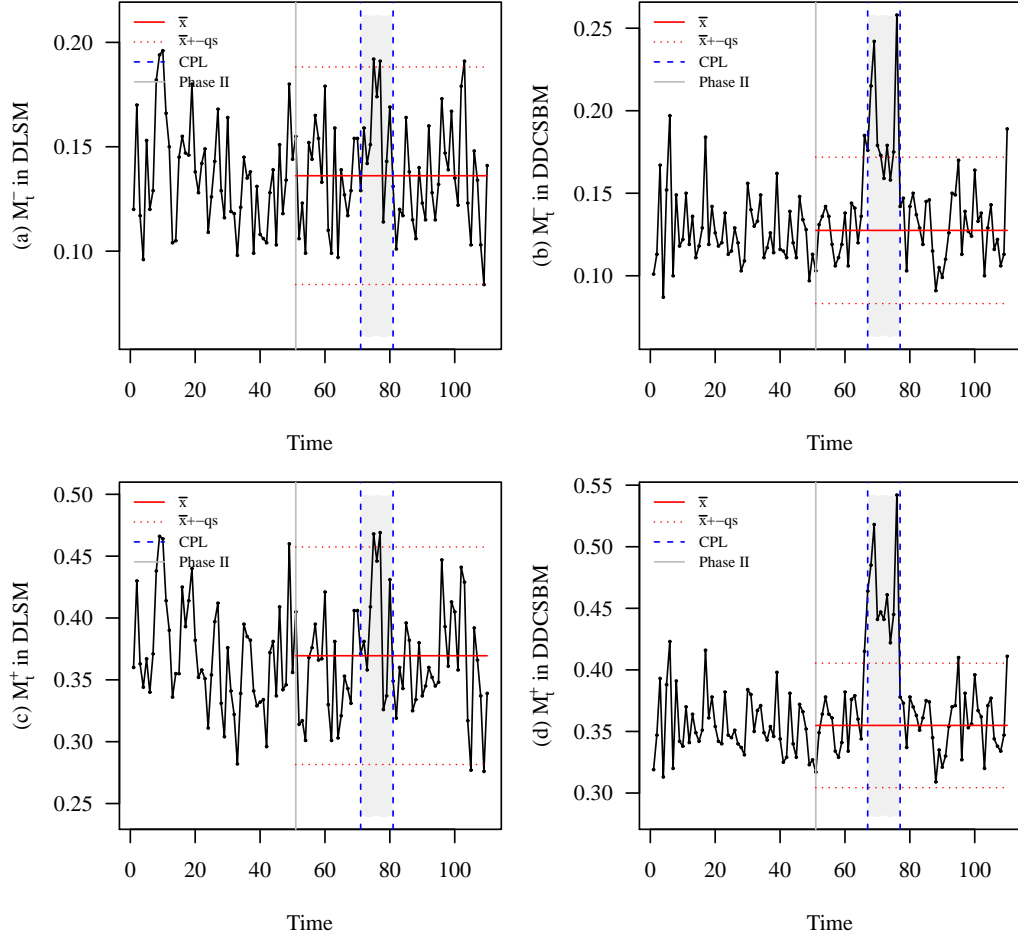


Figure 7: Shewhart Individuals Control Charts of M_t^- and M_t^+ for an Anomaly in Edge Probabilities in Binary Settings with $\phi = 0.5$ and $E[W_t] = 0.11$. Plots (a) and (c) show M_t^- and M_t^+ in a DLSDM setting, and plots (b) and (d) show M_t^- and M_t^+ in a DDCSBM setting. Limits q are determined setting empirical conditional false alarm probabilities at 0.03.

in DDCSBM settings. The worst monitoring performance, as might be expected, is S_t^* across all settings with a decrease in AUC of about 10% to 40% compared to other summary statistics. Across duration of anomaly (CPL) and correlation (ϕ), there is little difference in AUC values. However, sparsity ($E[W_t]$) has some effect since the sparser the network, the more difficult it could be to detect an anomaly.

Table 5: DR for DLSD with 33 Anomalous Nodes and OR from 1 to 4.

Settings			Binary					Count				
CPL	ϕ	$E[W_t]$	W_t	D_t	M_t^-	M_t^+	S_t^*	W_t	D_t	M_t^-	M_t^+	S_t^*
5	0.5	0.11	0.320	0.365	0.400	0.365	0.210	0.980	1	1	1	0.545
10	0.5	0.11	0.560	0.605	0.595	0.605	0.405	0.995	1	1	1	0.560
15	0.5	0.11	0.700	0.775	0.730	0.745	0.460	1	1	1	1	0.545
10	0.1	0.11	0.540	0.650	0.635	0.590	0.365	1	1	1	1	0.630
10	0.9	0.11	0.340	0.480	0.515	0.450	0.275	0.920	1	1	1	0.290
10	0.5	0.03	0.530	0.470	0.430	0.520	0.350	0.900	0.970	0.970	0.970	0.630
10	0.5	0.21	0.530	0.725	0.780	0.680	0.340	0.990	1	1	1	0.850

Table 6: DR for DLSD with 79 Anomalous Nodes and OR from 1 to 2.5.

Settings			Binary					Count				
CPL	ϕ	$E[W_t]$	W_t	D_t	M_t^-	M_t^+	S_t^*	W_t	D_t	M_t^-	M_t^+	S_t^*
5	0.5	0.11	0.955	0.940	0.685	0.940	0.645	1	1	1	1	0.985
10	0.5	0.11	0.990	0.985	0.870	0.990	0.660	1	1	1	1	0.985
15	0.5	0.11	1	0.995	0.925	0.995	0.725	1	1	1	1	0.975
10	0.1	0.11	0.995	0.990	0.840	0.990	0.715	1	1	1	1	0.990
10	0.9	0.11	0.880	0.860	0.740	0.870	0.360	1	1	1	1	0.930
10	0.5	0.03	1	0.810	0.635	0.890	0.500	1	1	0.99	1	0.775
10	0.5	0.21	1	1	0.935	1	0.755	1	1	1	1	0.975

Table 7: DR for DDCSBM with 33 Anomalous Nodes and OR from 1 to 2.5.

Settings			Binary					Count				
CPL	ϕ	$E[W_t]$	W_t	D_t	M_t^-	M_t^+	S_t^*	W_t	D_t	M_t^-	M_t^+	S_t^*
5	0.5	0.11	1	0.825	0.605	0.925	0.695	1	0.915	0.755	0.970	0.760
10	0.5	0.11	1	0.945	0.820	0.995	0.730	1	0.985	0.930	1	0.795
15	0.5	0.11	1	0.980	0.905	0.995	0.790	1	1	0.985	1	0.785
10	0.1	0.11	1	0.950	0.835	0.990	0.780	1	0.990	0.970	1	0.800
10	0.9	0.11	1	0.925	0.825	0.990	0.610	1	0.990	0.955	0.995	0.650
10	0.5	0.03	0.99	0.780	0.665	0.855	0.630	0.985	0.820	0.745	0.880	0.540
10	0.5	0.21	1	0.985	0.830	0.995	0.960	1	0.995	0.980	1	0.995

Table 8: DR for DDCSBM with 72 Anomalous Nodes and OR from 1 to 1.5.

Settings			Binary					Count				
CPL	ϕ	$E[W_t]$	W_t	D_t	M_t^-	M_t^+	S_t^*	W_t	D_t	M_t^-	M_t^+	S_t^*
5	0.5	0.11	1	0.885	0.560	0.995	0.870	1	0.930	0.670	0.990	0.860
10	0.5	0.11	1	0.990	0.820	1	0.925	1	0.985	0.830	1	0.915
15	0.5	0.11	1	1	0.915	1	0.890	1	0.985	0.915	1	0.915
10	0.1	0.11	1	0.990	0.835	1	0.865	1	0.990	0.910	0.995	0.920
10	0.9	0.11	1	0.985	0.800	1	0.870	1	0.985	0.890	0.995	0.820
10	0.5	0.03	1	0.855	0.685	0.940	0.720	1	0.835	0.665	0.970	0.715
10	0.5	0.21	1	0.995	0.805	1	1	1	1	0.910	1	1

The scenarios considered thus far involved sustained anomalies in network density. Now, we compare such an anomaly with one that gradually increases network density over the duration of the anomaly or CPL. In the next set of scenarios, the odds ratio is gradually increased from 1 to 12 in a DLISM network and from 1 to 3.5 in a DDCSBM network for a sub-network of 39 nodes. When only varying CPL, CPL varies from 15, 20, to 25. For all other settings, CPL is 20.

DR results are reported in Tables 9 and 10 below with AUC results in Tables 22 and 23 in Appendix A.3. The values of the best monitoring performances are in bold, and in cases with a gradual change in the odds ratio, we see monitoring W_t , D_t , M_t^- , and M_t^+ all detect this embedded anomaly well. The scan statistic method detects less well in binary cases and rather well in count settings. AUC Results from Tables 22 and 23 in Appendix A.3 are fairly similar to the sustained changes in odds ratio. Therefore, between sustained and gradual changes, monitoring M_t^+ does best in most DLISM settings while monitoring W_t detects best in DDCSBM settings with respect to DR and AUC.

Table 9: DR for DLISM with 39 Anomalous Nodes with $OR \in [1, 12]$.

Settings			Binary					Count				
CPL	ϕ	$E[W_t]$	W_t	D_t	M_t^-	M_t^+	S_t^*	W_t	D_t	M_t^-	M_t^+	S_t^*
15	0.5	0.11	0.920	0.990	0.985	0.990	0.550	1	1	1	1	0.975
20	0.5	0.11	0.965	0.985	0.985	0.985	0.645	1	1	1	1	0.975
25	0.5	0.11	0.965	1	1	1	0.665	1	1	1	1	0.985
20	0.1	0.11	0.980	0.995	0.990	0.995	0.675	1	1	1	1	0.965
20	0.9	0.11	0.735	0.955	0.955	0.910	0.520	1	1	1	1	0.735
20	0.5	0.03	0.945	0.920	0.880	0.950	0.510	1	1	1	1	0.955
20	0.5	0.21	0.980	1	1	1	0.655	1	1	1	1	0.980

Table 10: DR for DDCSBM with 39 Anomalous Nodes with $OR \in [1, 3.5]$.

Settings			Binary					Count				
CPL	ϕ	$E[W_t]$	W_t	D_t	M_t^-	M_t^+	S_t^*	W_t	D_t	M_t^-	M_t^+	S_t^*
15	0.5	0.11	1	1	1	1	0.830	1	1	1	1	0.920
20	0.5	0.11	1	1	0.995	1	0.880	1	1	1	1	0.940
25	0.5	0.11	1	1	1	1	0.880	1	1	1	1	0.865
20	0.1	0.11	1	1	1	1	0.910	1	1	1	1	0.915
20	0.9	0.11	1	1	0.995	1	0.710	1	1	1	1	0.815
20	0.5	0.03	1	0.985	0.970	1	0.775	1	0.985	0.96	1	0.815
20	0.5	0.21	1	1	0.995	1	0.965	1	1	1	1	0.990

4.5 Performance Evaluation with Anomalies in Expected Degree

In attempts to manipulate maximum degree, we target effects of parameters in a DLSM and DDCSBM related to degree(s) of a node(s), which mainly affect expected degree. Such parameters are r_i in a DLSM, which represents a radius of communication in the latent space for node i that indirectly affects degree, and θ_{it} in a DDCSBM, which represents a propensity for node i to communicate at time t that directly affects degree. Recall, propensities of communication are a degree-correction for the stochastic block model. First note that having radii in a DLSM be time dependent neither drastically changes nor improves model fitting as discussed by Sewell and Chen (2015). Second note that correlation via time in a DLSM is incorporated via latent positions and not r_i , whereas correlation via time for a DDCSBM is through degree parameters, Θ . By manipulating degree parameters directly in a DDCSBM model, we cannot simply change the value of θ_i at anomalous time points. Rather, θ_{it} is multiplied by some constant, C , throughout the anomalous time period. Table 11 summarizes considered scenarios affecting a certain number of nodes and the settings for model parameters. For a DLSM, r_i are directly manipulated for a binary (B) and count (C) network, while in a DDCSBM, θ_{it} are multiplied by some constant C . Shift size indicates a medium or large change in expected degrees.

Shift Size	Number of Nodes (N)	$r_i = 0.1$ to	$C \cdot \Theta$ $C = 1$ to
Medium	15	0.020(B);0.04(C)	2.25
Large	35	0.015(B);0.0225(C)	1 .75

Table 11: Scenarios for Simulation Study Targeting Max Degree via Node Parameters.

Recall, N denotes the number of nodes affected by a given change. An example using $N = 15$ with $r_i = 0.04$ is shown in a count DLSM in Figure 8 with $\phi = 0.5$, $E[W_t] = 0.11$, and settings mentioned in Section 4.1. In Figure 8, the $N = 15$ affected nodes are enlarged and colored red with only the associated edges to and from those nodes displayed in red as well. An increase in communication among the $N = 15$ nodes can be viewed during an anomalous time within the change point interval. Note, while edge probabilities of these nodes are affected by manipulating expected degree during each time-point of the change point interval, not all time-points during the

anomaly will have such an increase in communication as this example. Shewhart control charts for this example are plotted for W_t and D_t with Phase I data for $t \leq 50$ in Figure 9. In this example, the network density chart signals a decrease in network density in the DLSM setting, Figure 9 (a). Figures 9 (c) and (d) show D_t signaling during the change point interval along with some false alarms.

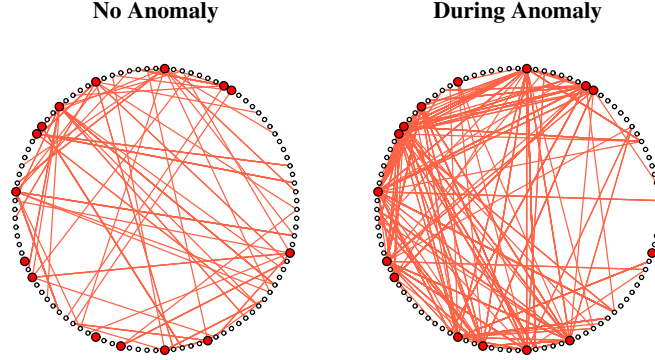


Figure 8: Edges of 15 Nodes in Count DLSM Networks (a) Before and (b) During an Anomaly Targeting Max Degree. A subset of 15 nodes (large red vertices) have $r_i = 0.01$ increased to $r_i = 0.04$ for the anomaly. Only edges from those 15 nodes are displayed, and an increase in communication for those 15 nodes is observed.

Results of 200 simulations with $n = 100$, $T = 110$, and $CPL = 5, 10$, or 15 are summarized below in Tables 12 - 15 using DR and in Appendix A.4 Tables 18 -21 using AUC. The best value of the metric is in bold. Since anomalies planted affect expected degree (and desirably maximum degree), a natural best method would be D_t . As with anomalies in edge probabilities, results are explained first by model and network type settings and then across trends in CPL, correlation, and sparsity. In nearly all of DLSM and DDCSBM settings, use of M_t^- yields the highest detection rates. In the medium shift size count DLSM settings, monitoring D_t and M_t^+ detect just about as well. In medium shift size DDCSBM settings, D_t , M_t^- , and M_t^+ methods all detect perfectly with a DR of 1. Detection rates across the board in the large shift size case (many nodes with a slight increase in expected degree) tend to be lower than the medium shift size case (some nodes with an increase in expected degree). This finding suggests detecting a change with some nodes affecting expected degree is easier than when many nodes affect expected degree. The worst monitoring performance in all scenarios is W_t , with the highest DR of 35%. The second worst performing method is S_t^* , but it performs especially well in a count DLSM with a longer CPL and a count DDCSBM with a medium shift size. There is noticeably less effect from duration, correlation, and sparsity for most statistics. However, the scan statistic appears to be detect better with a longer CPL in DLSM settings. In general, most methods other than W_t have high detection rates when planting an anomaly in expected degree. Unlike in the case where anomalies are embedded in edge probabilities, detection rates in DDCSBM count settings are better.

In AUC results reported in Tables 24 -27 in Appendix A.4, the detection ability is mainly best for M_t^- and D_t methods in both DLSM and DDCSBM settings. The worst monitoring performance is W_t with second worst being S_t^* across all settings. In general, W_t and S_t^* methods suffer about a 30% to 60% loss in AUC compared to other summary statistics. Across duration of anomaly (CPL) and correlation (ϕ), there is little difference in AUC values. It appears to be difficult to

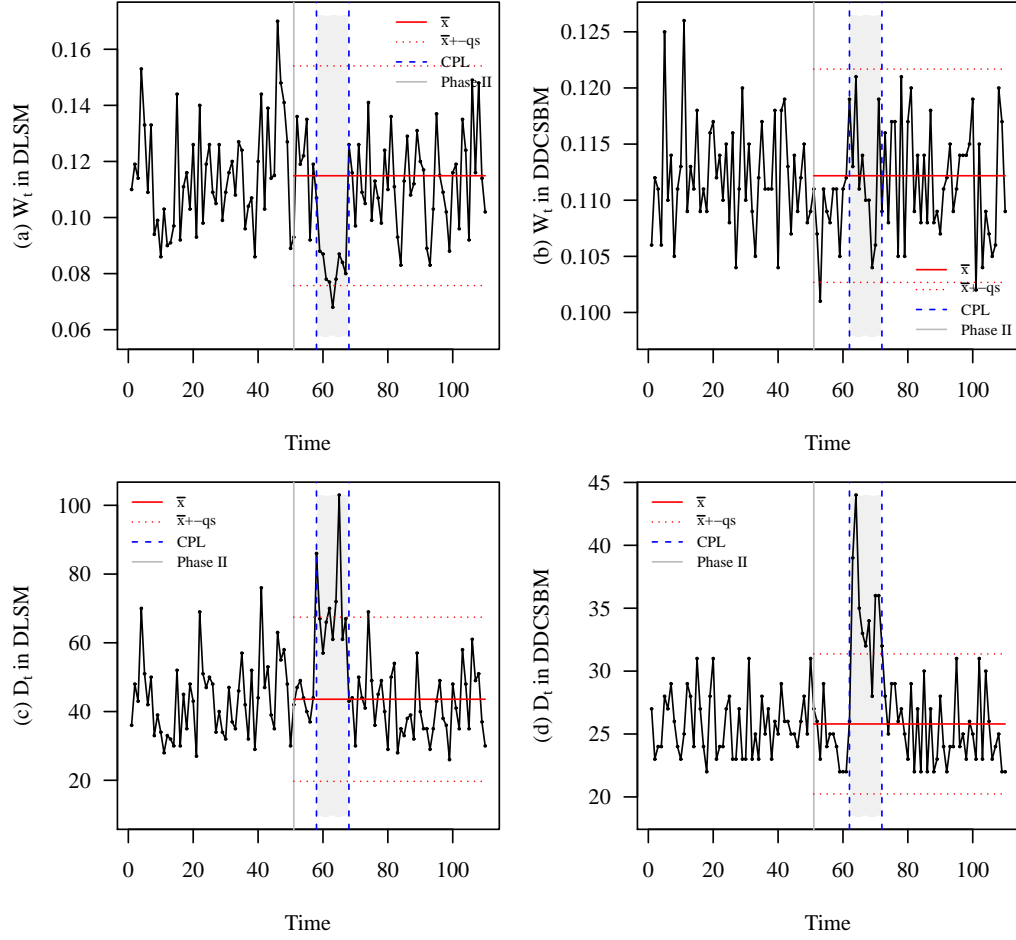


Figure 9: Shewhart Individuals Control Charts of W_t and D_t for an Anomaly Targeting Expected Degree in Count Settings with $\phi = 0.5$ and $E[W_t] = 0.11$. Plots (a) and (c) show W_t and D_t in a DLSM setting, and plots (b) and (d) show W_t and D_t in a DDCSBM setting. Limits q are determined setting empirical conditional false alarm probabilities at 0.03.

detect an anomaly when there is less communication (greater sparsity) in the network. For AUC values, DLSM count settings tend to have lower AUC than in DLSM binary settings.

Table 12: DR for DLSDM from $r_i = 0.1$ to $r_i = 0.020$ (B); 0.04 (C) for $N = 15$.

Settings			Binary					Count				
CPL	ϕ	$E[W_t]$	W_t	D_t	M_t^-	M_t^+	S_t^*	W_t	D_t	M_t^-	M_t^+	S_t^*
5	0.5	0.11	0.045	1	1	0.995	0.375	0.00	0.990	1	0.985	0.380
10	0.5	0.11	0.130	1	1	0.995	0.460	0.01	1	1	1	0.690
15	0.5	0.11	0.120	1	1	1	0.630	0.02	1	1	1	0.845
10	0.1	0.11	0.115	1	1	1	0.530	0.01	1	1	1	0.610
10	0.9	0.11	0.055	0.990	1	0.930	0.500	0.01	0.995	0.995	0.960	0.685
10	0.5	0.03	0.175	0.995	1	0.970	0.440	0.07	0.905	0.940	0.845	0.780
10	0.5	0.21	0.065	1	1	1	0.425	0.00	1	1	1	0.630

Table 13: DR for DLSDM from $r_i = 0.1$ to $r_i = 0.015$ (B); 0.0225 (C) for $N = 35$.

Settings			Binary					Count				
CPL	ϕ	$E[W_t]$	W_t	D_t	M_t^-	M_t^+	S_t^*	W_t	D_t	M_t^-	M_t^+	S_t^*
5	0.5	0.11	0.095	0.970	1	0.845	0.345	0.065	0.940	0.995	0.860	0.465
10	0.5	0.11	0.130	0.980	1	0.920	0.530	0.075	0.995	1	0.960	0.655
15	0.5	0.11	0.220	0.995	1	0.965	0.620	0.120	1	1	0.980	0.945
10	0.1	0.11	0.085	1	1	0.955	0.465	0.095	0.975	0.990	0.945	0.715
10	0.9	0.11	0.055	0.940	1	0.805	0.430	0.050	0.950	0.990	0.890	0.680
10	0.5	0.03	0.205	0.930	0.950	0.865	0.495	0.165	0.745	0.770	0.705	0.680
10	0.5	0.21	0.060	0.995	1	0.865	0.375	0.030	1	1	0.985	0.600

Table 14: DR for DDCSBM from $C = 1$ to $C = 2.25$ in $C \cdot \Theta$ for $N = 15$.

Settings			Binary					Count				
CPL	ϕ	$E[W_t]$	W_t	D_t	M_t^-	M_t^+	S_t^*	W_t	D_t	M_t^-	M_t^+	S_t^*
5	0.5	0.11	0.085	1	1	1	0.770	0.245	1	1	1	0.835
10	0.5	0.11	0.155	1	1	1	0.780	0.195	1	1	1	0.845
15	0.5	0.11	0.130	1	1	1	0.810	0.285	1	1	1	0.850
10	0.1	0.11	0.115	1	1	1	0.770	0.285	1	1	1	0.840
10	0.9	0.11	0.140	0.990	0.995	0.990	0.735	0.185	1	1	1	0.800
10	0.5	0.03	0.330	0.990	0.990	0.985	0.580	0.340	0.990	0.995	0.975	0.620
10	0.5	0.21	0.090	1	1	1	0.850	0.170	1	1	1	0.900

Table 15: DR for DDCSBM from $C = 1$ to $C = 1.75$ in $C \cdot \Theta$ for $N = 35$.

Settings			Binary					Count				
CPL	ϕ	$E[W_t]$	W_t	D_t	M_t^-	M_t^+	S_t^*	W_t	D_t	M_t^-	M_t^+	S_t^*
5	0.5	0.11	0.145	0.950	0.965	0.935	0.585	0.255	0.985	0.985	0.985	0.625
10	0.5	0.11	0.215	0.975	0.990	0.965	0.625	0.285	0.990	0.990	0.990	0.635
15	0.5	0.11	0.245	1	1	0.985	0.650	0.350	0.990	0.995	0.990	0.715
10	0.1	0.11	0.185	0.970	0.970	0.955	0.650	0.280	0.995	0.995	0.985	0.665
10	0.9	0.11	0.165	0.985	0.990	0.975	0.560	0.330	0.990	1	0.990	0.565
10	0.5	0.03	0.330	0.845	0.855	0.815	0.530	0.395	0.835	0.860	0.850	0.570
10	0.5	0.21	0.075	0.980	0.990	0.965	0.630	0.285	0.995	1	0.995	0.690

As before with anomalies within edge probabilities, we compare sustained changes in expected degree to a gradual increase of expected degree over the duration of the anomaly (CPL). In this last set of scenarios, r_i is increased from $r_i = 1/n$ to $4/n$ in a DLSDM setting and C is increased from $C = 1$ to 5 in a DDCSBM setting.

DR results are reported in Tables 16 and 17 with AUC results in Tables 28 and 29 in Appendix A.4. Similar to the sustained change case, M_t^- and D_t methods detect this change the best in DLSDM settings. However, monitoring D_t , M_t^- , and M_t^+ all detect perfectly with a DR of 1 in DDCSBM settings. The worst monitoring performance is with W_t , and scan statistics detect more poorly in DLSDM settings than in DDCSBM settings. One reason S_t^* method might be performing poorly is because of window contamination as discussed in Zhao et al. (2018b). Since the same subset of nodes are increasing slowly in expected degree, this effect can be captured in a given window and subsequent moving windows. Thus, the standardization process will have already included the anomaly, which makes detecting a gradual change much more difficult. In DDCSBM settings, the same possible window contamination does not affect detection rates as in DLSDM settings. AUC results are in Tables 28 and 29 in Appendix A.4. The best monitoring performance with respect to AUC is M_t^- for targeting anomalies that are aimed to affect maximum degree. As seen in the sustained case in DLSDM settings, changes in radii are not as impactful as in count networks. In some instances, AUC increases, but in others, it decreases. For DDCSBM settings, count networks tend to have higher AUC than in binary networks, which suggests the loss of information in binary networks makes the change slightly harder to detect.

Table 16: DR for DLSM from $r_i \in [1/n, 4/n]$ for $N = 20$.

Settings			Binary					Count				
CPL	ϕ	$E[W_t]$	W_t	D_t	M_t^-	M_t^+	S_t^*	W_t	D_t	M_t^-	M_t^+	S_t^*
15	0.5	0.11	0.065	1	1	0.890	0.250	0.110	0.955	0.985	0.910	0.345
20	0.5	0.11	0.095	1	1	0.910	0.305	0.170	0.975	0.995	0.950	0.410
25	0.5	0.11	0.135	1	1	0.970	0.300	0.175	0.995	0.995	0.975	0.465
20	0.1	0.11	0.090	1	1	0.945	0.345	0.185	0.995	1	0.975	0.400
20	0.9	0.11	0.060	0.98	1	0.730	0.320	0.100	0.990	0.995	0.935	0.485
20	0.5	0.03	0.150	1	1	0.985	0.440	0.245	0.790	0.795	0.720	0.490
20	0.5	0.21	0.050	1	1	0.735	0.165	0.180	0.995	0.995	0.985	0.365

Table 17: DR for DDCSBM from $C \in [1, 5]$ in $C \cdot \Theta$ for $N = 20$.

Settings			Binary					Count				
CPL	ϕ	$E[W_t]$	W_t	D_t	M_t^-	M_t^+	S_t^*	W_t	D_t	M_t^-	M_t^+	S_t^*
15	0.5	0.11	0.065	1	1	1	0.825	0.180	1	1	1	0.865
20	0.5	0.11	0.135	1	1	1	0.825	0.170	1	1	1	0.865
25	0.5	0.11	0.110	1	1	1	0.770	0.195	1	1	1	0.825
20	0.1	0.11	0.105	1	1	1	0.775	0.155	1	1	1	0.855
20	0.9	0.11	0.120	1	1	1	0.685	0.205	1	1	1	0.815
20	0.5	0.03	0.265	1	1	1	0.710	0.310	1	1	1	0.760
20	0.5	0.21	0.080	1	1	1	0.700	0.110	1	1	1	0.830

4.6 Overall summary of results

In the light of the results from our performance evaluation study, we make the following general observations:

1. Summary statistics like network density, maximum degree, and their linear combinations can be valuable and effective monitoring tools for detecting anomalous changes in time-evolving networks. In particular, such summary statistics can be much more powerful than more complicated and computationally expensive monitoring techniques like the scan statistic of Priebe et al. (2005). This remarkable fact is demonstrated throughout our study and establishes the value of using summary statistics in network monitoring.
2. Network density (W_t) is effective in detecting changes in the odds ratio (Tables 5–10), but ineffective in detecting changes in individual node behavior (Tables 12–17). This is consistent with what one would expect, as changes in individual node behavior do not significantly affect the overall network density.
3. Maximum degree (D_t) is effective in detecting changes in individual node behavior (Tables 12–17), which is expected. In addition, maximum degree is also effective in detecting changes

in odds ratio (Tables 5–10), often performing close to or better than network density. This makes maximum degree a versatile summary statistic for network monitoring.

4. The linear combinations (M_t^- and M_t^+) can combine the strengths of network density and maximum degree. For example, when the anomaly corresponds to an increase in the odds ratio, there is an increase in both network density and maximum degree. In such cases, the detection rates of M_t^+ are often higher than maximum degree (Tables 5–10). Furthermore, when the anomaly consists of change in individual node behavior, the detection rates of M_t^- and M_t^+ are much higher than network density (Tables 12–17).
5. Another way to combine the strengths of network density and maximum degree would be to consider (W_t, D_t) as a bivariate summary statistic and employ bivariate process monitoring methods. To accomplish this, we need to consider the covariance between W_t and D_t and update the calibration of \bar{x} , s , and q accordingly to construct bivariate control limits. This seems to be a very promising approach that we plan to explore in future work.

5 Conclusion

Anomaly detection in temporally-evolving networks is an active area of research, but often subject to a specific network model. In this work, we explored network monitoring approaches on calculated summary statistics using a comprehensive simulation study. Performance evaluations of summary statistics, density, maximum degree, and linear combinations of density and maximum degree, were compared to that of the scan statistic. To introduce interesting complexities, temporally-evolving network models, DLSMs and DDCSBMs, were used to incorporate correlation over time. This correlation better models phenomena in time-varying networks as opposed to independent snapshots over time.

In evaluating performance, metrics such as detection rates and area under a receiver-operating curve suggest that simple, relatively easy-to-compute summary statistics can outperform the more sophisticated, difficult-to-implement scan method. Albeit, the measures of success analyzed may not be best suited for documenting the advantages of a scan statistic. The scan statistic is, by construct, vulnerable to missing gradual changes in networks, i.e., window contamination. The types of planted anomalies in our simulations resulted from intentional changes in edge probabilities and expected degree. Specifically, adjustments were made to the odds ratios of edge probabilities and model parameters governing expected degree. While use of W_t performs better to detect anomalies resulting from changes in edge probabilities, W_t method performed the worst with anomalies concerning expected degree. Use of maximum degree (D_t), however, does fairly well in both scenarios, yet use of linear combinations of W_t and D_t , M_t^- and M_t^+ , perform the best in both scenarios.

To summarize, this paper demonstrates that monitoring summary statistics has clear advantages. They are simple to calculate, easy to interpret, and able to catch several types of anomalies. Based on results from a detailed simulation study, summary statistics showed effective in detecting anomalies under varying conditions pertaining to the following: anomaly duration, correlation, sparsity, network types, and network models. Admittedly, summary statistics will not detect some anomalies that do not impact the statistics directly; e.g., extreme-node-switching, where two nodes that have, say, the maximum degree and minimum degrees in a network at time t , swap at time $t + 1$. To detect such an anomaly would require detailed modeling efforts, whereas the model-free approach presented here with summary statistics saves time and fosters consistency across efforts in

detecting anomalies. However, we might improve the effectiveness of monitoring summary statistics by considering multivariate, rather than univariate analytic approaches; i.e., at time t , assessing density (W_t), maximum degree (D_t), difference (M_t^-), and/or sum (M_t^+) jointly. In future work, generalizing univariate methods to multivariate methods should be considered.

Lastly, efforts in this paper concentrated on performance evaluation assessment of summary statistics by using simulated network data. These network monitoring methods can be easily applied to non-synthesized data as a first step in anomaly detection. A few issues arise when utilizing a process monitoring application. One issue is determining the number of time-points for Phase I data since control limits need to be estimated accurately. Another issue is being reasonably sure that no anomalies occurred in Phase I. Any anomalies in Phase I data would be incorrectly incorporated as expected behavior. After control limits are established from Phase I data, monitoring begins in Phase II. If any anomalies are detected using network monitoring methods, then further investigation is needed to find a root cause. Thus, network monitoring methods can provide preliminary analysis on any anomalies in the data.

A Simulations with No Anomaly Additional Figures

A.1 Supplemental Figures for Section 2.2.2

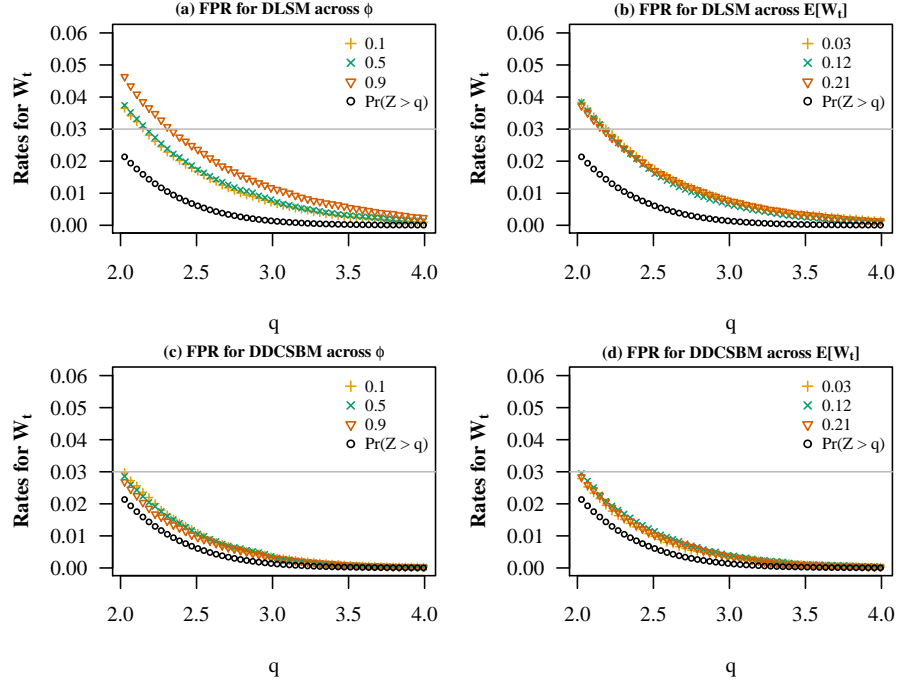


Figure 10: Plot of False Alarm Rates Monitoring W_t Across Varying Correlation [(a) and (c)] and Sparsity [(b) and (d)] in Count DSLM and DDSCSBM Settings.

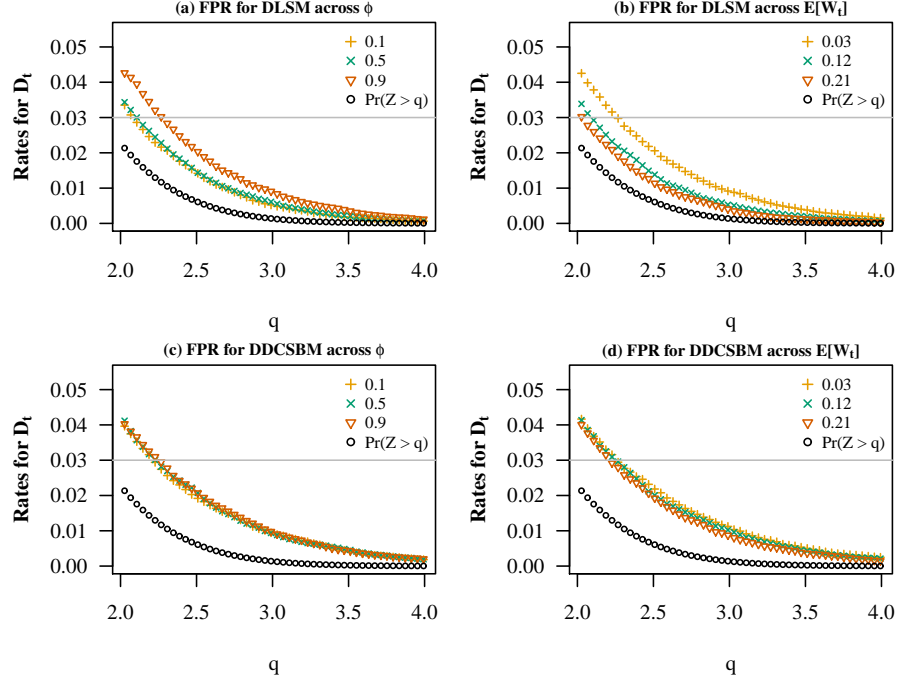


Figure 11: Plot of False Alarm Rates Monitoring D_t Across Varying Correlation [(a) and (c)] and Sparsity [(b) and (d)] Values in Binary DLSM and DDCSBM Settings.

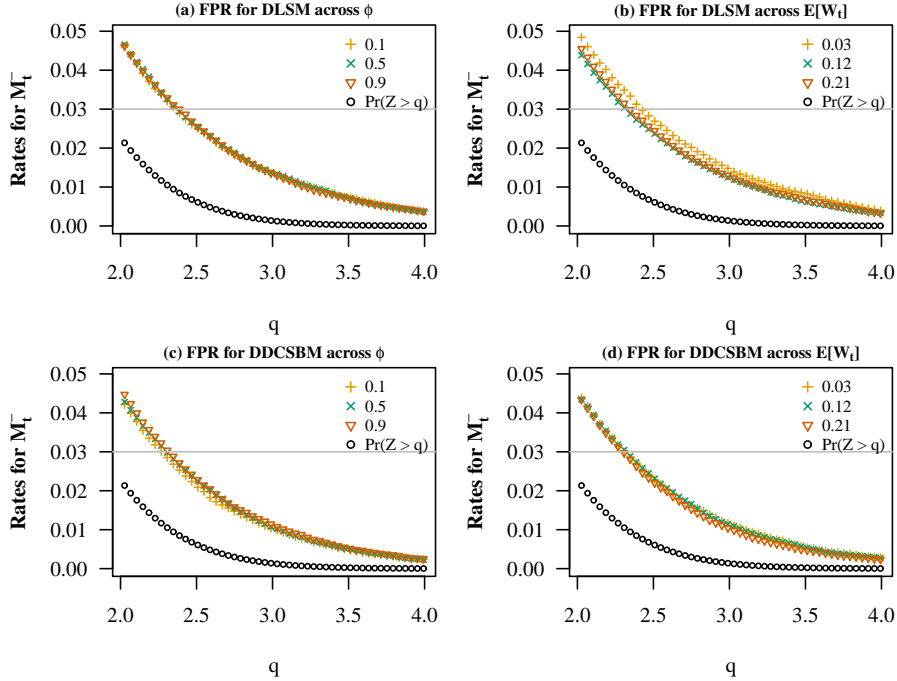


Figure 12: Plot of False Alarm Rates Monitoring M_t^- Across Varying Correlation [(a) and (c)] and Sparsity [(b) and (d)] Values in Count DLSM and DDCSBM Settings.

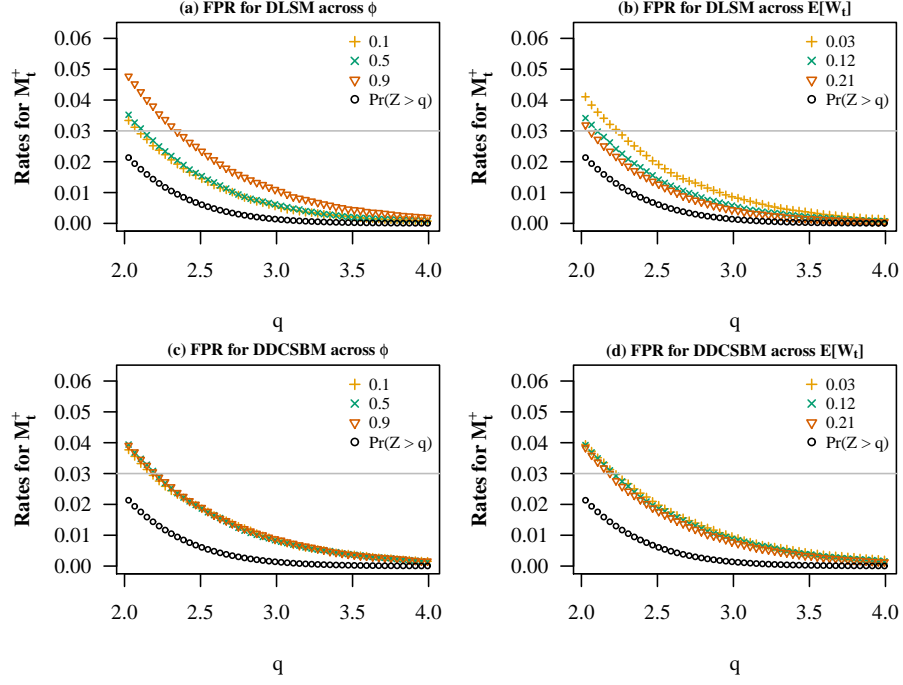


Figure 13: Plot of False Alarm Rates Monitoring M_t^+ Across Varying Correlation [(a) and (c)] and Sparsity [(b) and (d)] in Binary DSLM and DDCSBM Settings.

A.2 Supplemental Figures for Section 4.3

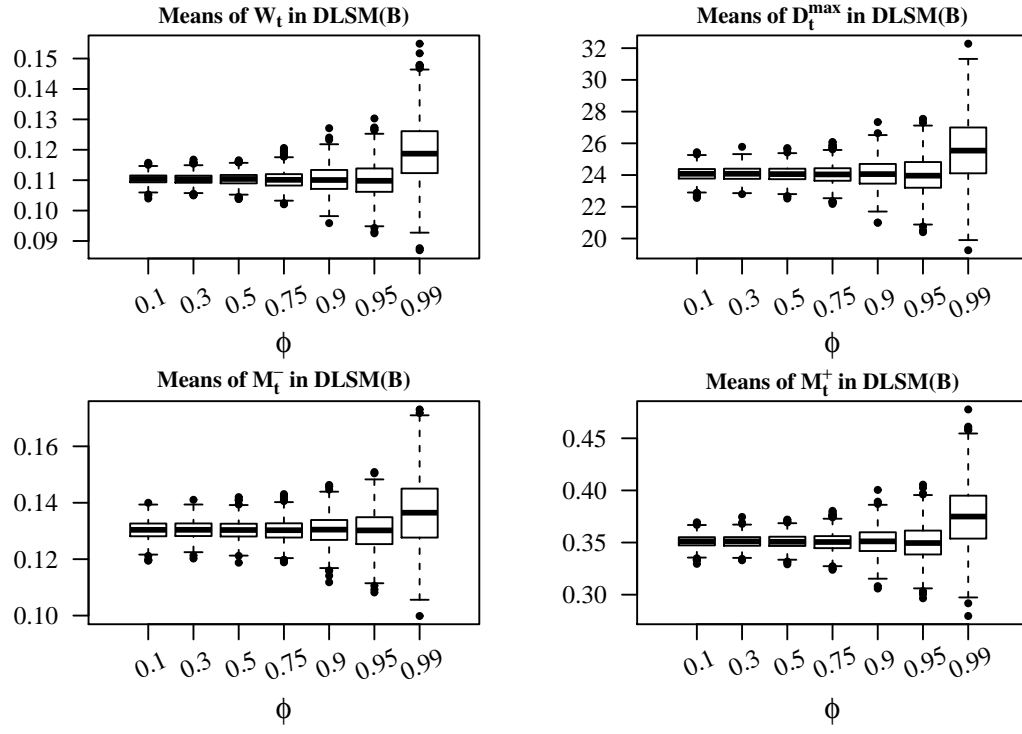


Figure 14: Plot of Means in a DLSD Binary (B) Setting Across Varying Correlation.

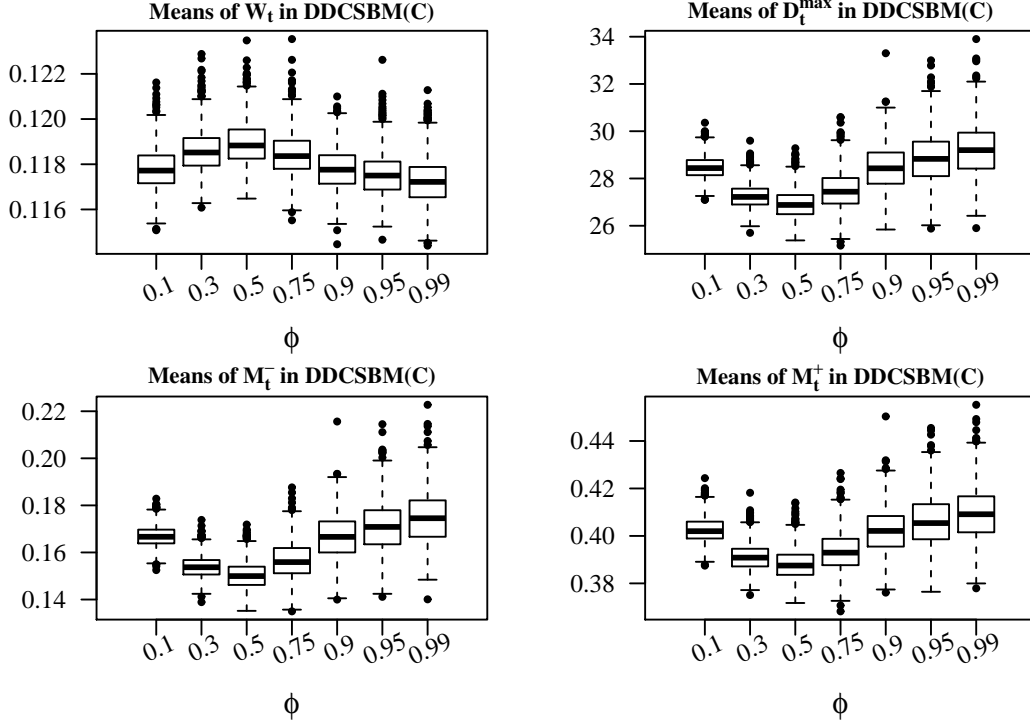


Figure 15: Plot of Means in a DDSCBM Count (C) Setting Across Varying Correlation.

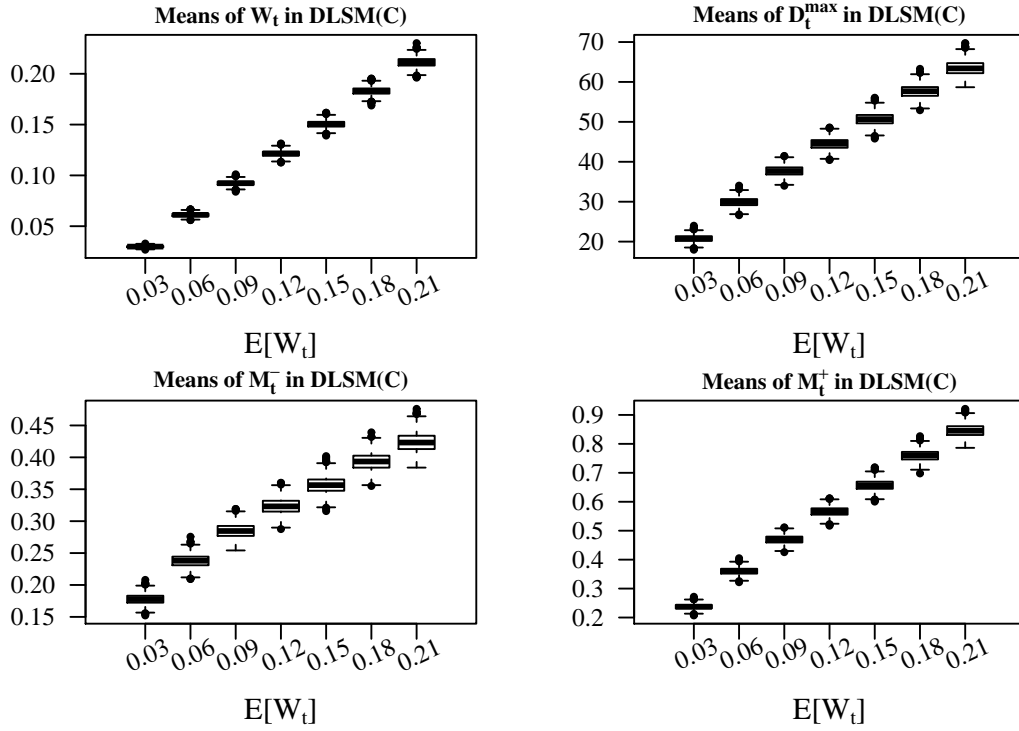


Figure 16: Plot of Means in a DLSC Count (C) Setting Across Varying Sparsity.

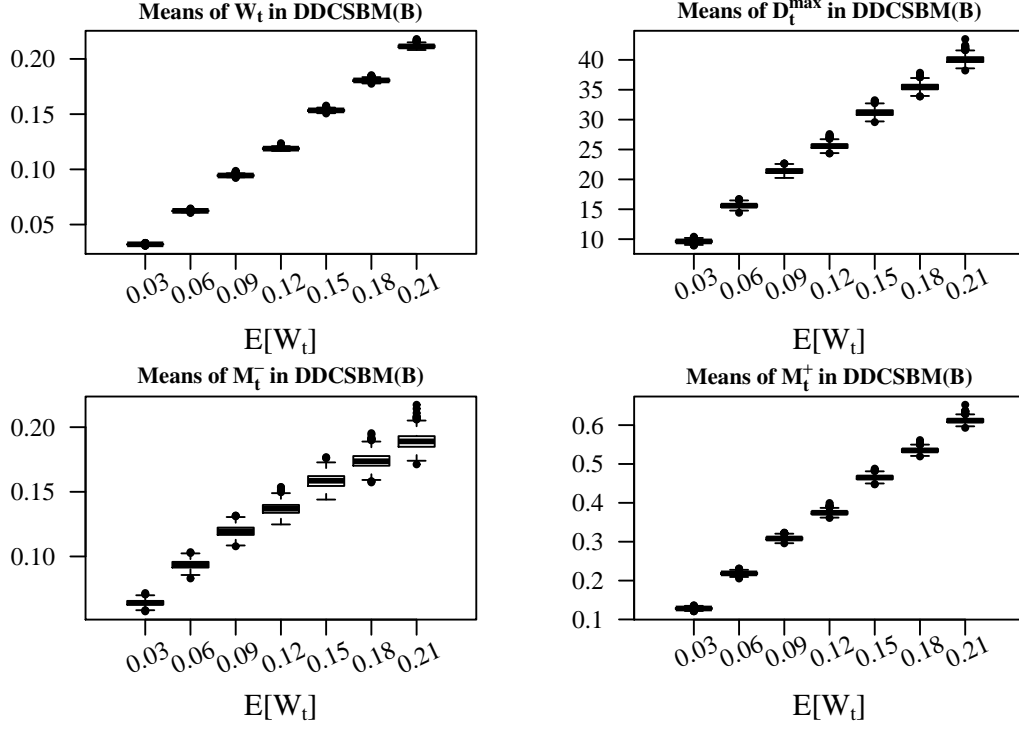


Figure 17: Plot of Means in a DDSCSBM Binary (B) Setting Across Varying Correlation.

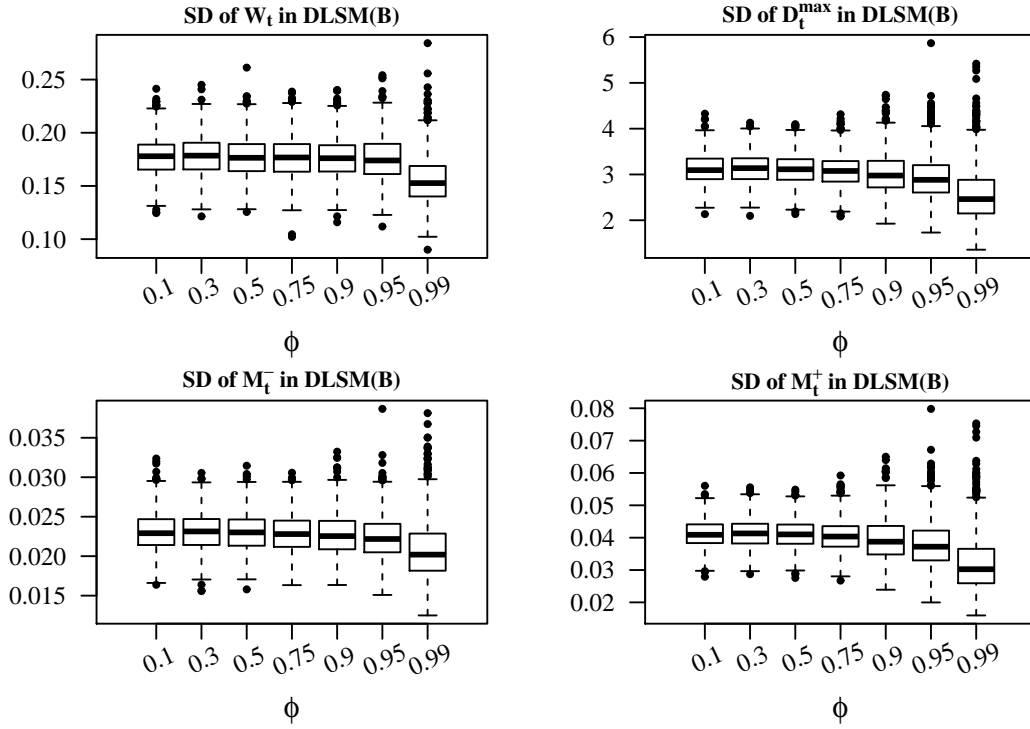


Figure 18: Plot of SD in a DLSCSBM Binary (B) Setting Across Varying Correlation.

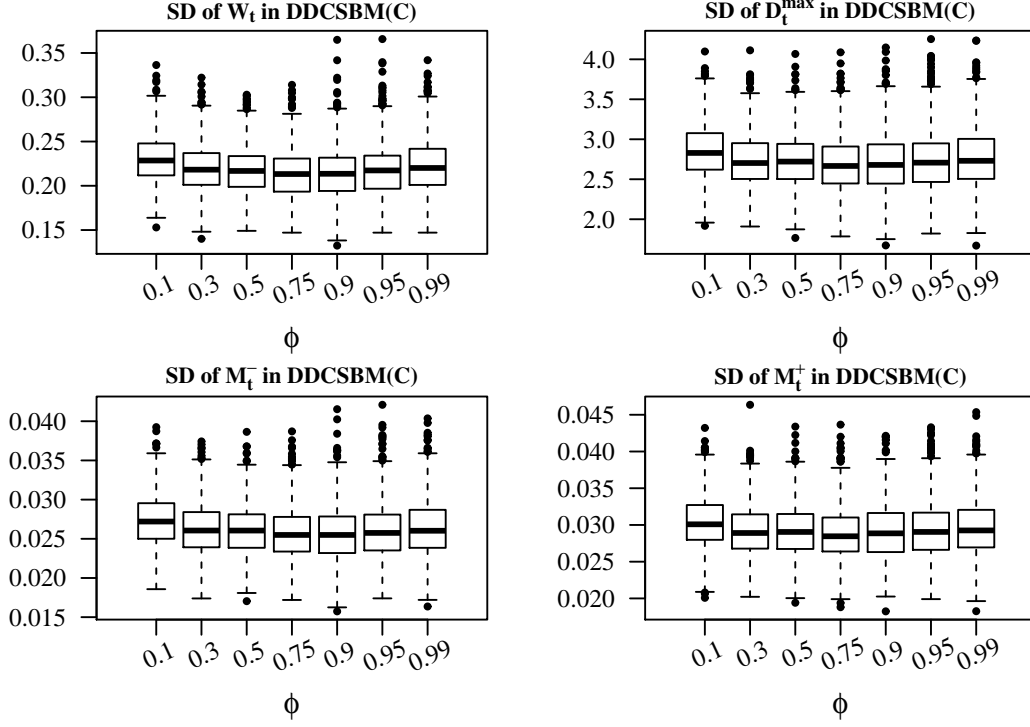


Figure 19: Plot of SD in a DDCSBM Count (C) Setting Across Varying Correlation.

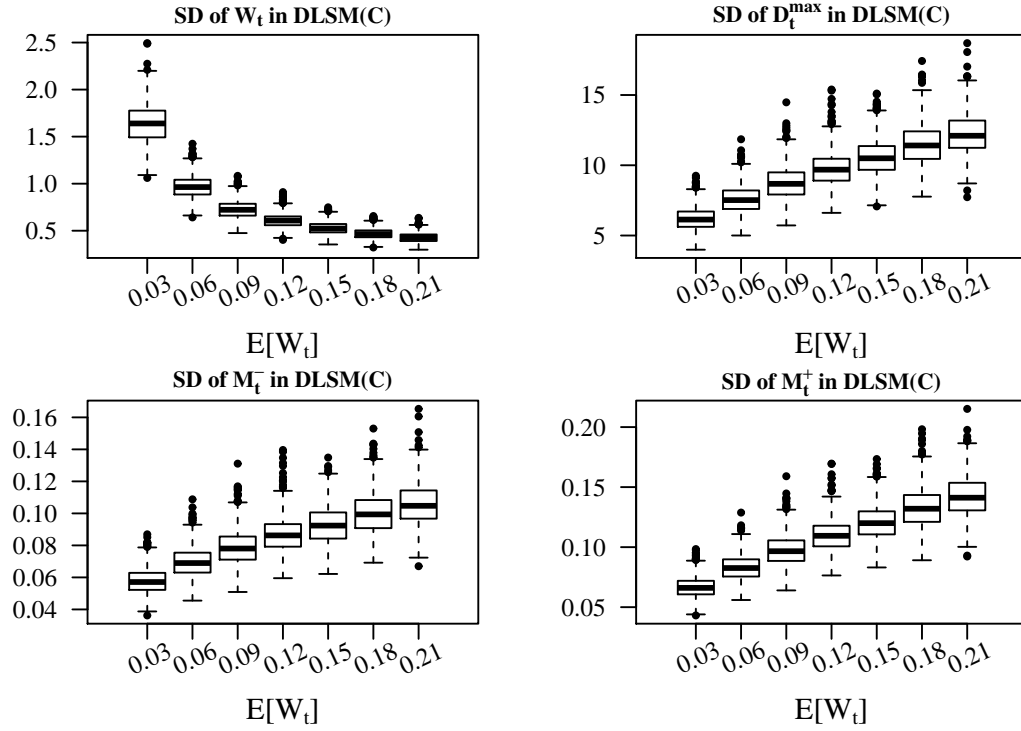


Figure 20: Plot of SD in a DLSDM Count (C) Setting Across Varying Sparsity.

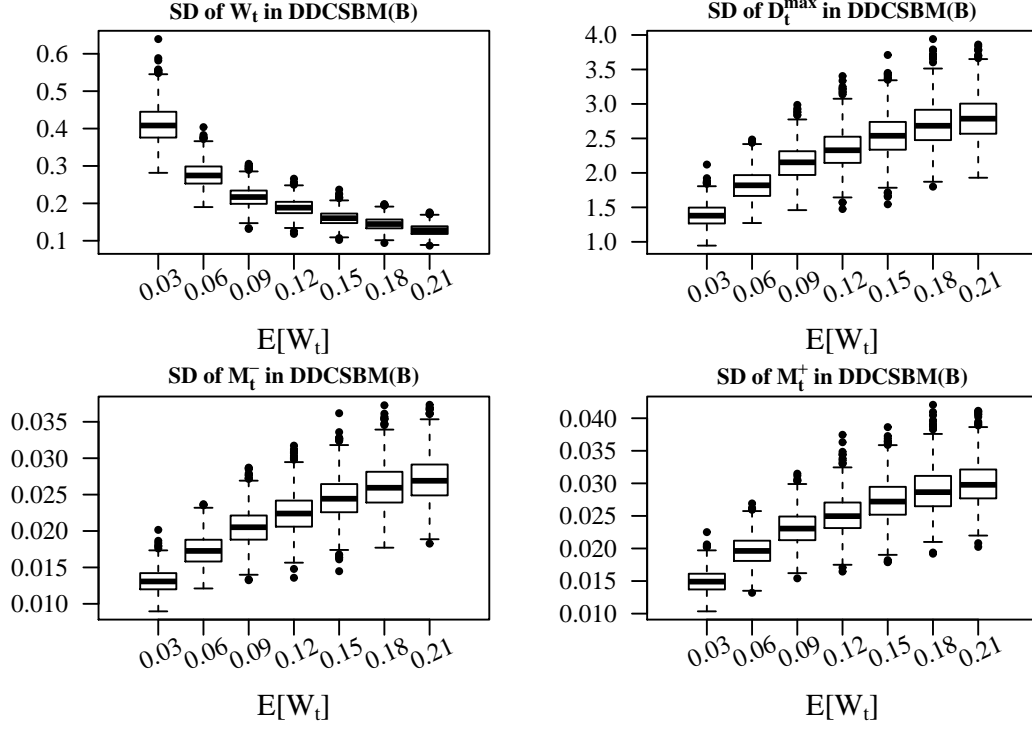


Figure 21: Plot of SD in a DDCSBM Binary (B) Setting Across Varying Correlation.

A.3 AUC Results for Section 4.4

Results of 200 simulations with $n = 100$, $T = 110$, and $CPL = 5, 10$, or 15 are summarized in Tables 18 -21 using AUC. The method which detects the embedded anomaly best are in bold.

Table 18: AUC for DLSP with 33 Anomalous Nodes and OR from 1 to 4.

Settings			Binary					Count				
CPL	ϕ	$E[W_t]$	W_t	D_t	M_t^-	M_t^+	S_t^*	W_t	D_t	M_t^-	M_t^+	S_t^*
5	0.5	0.11	0.649	0.667	0.648	0.670	0.598	0.937	0.992	0.994	0.990	0.877
10	0.5	0.11	0.641	0.664	0.652	0.665	0.584	0.933	0.994	0.995	0.991	0.768
15	0.5	0.11	0.658	0.665	0.645	0.671	0.547	0.935	0.993	0.994	0.991	0.681
10	0.1	0.11	0.652	0.667	0.648	0.672	0.576	0.933	0.993	0.995	0.990	0.759
10	0.9	0.11	0.695	0.697	0.668	0.705	0.546	0.936	0.993	0.994	0.991	0.667
10	0.5	0.03	0.645	0.615	0.595	0.629	0.554	0.727	0.751	0.745	0.755	0.618
10	0.5	0.21	0.655	0.720	0.723	0.707	0.570	0.871	0.937	0.932	0.938	0.706

Table 19: AUC for DLSP with 79 Anomalous Nodes and OR from 1 to 2.5.

Settings			Binary					Count				
CPL	ϕ	$E[W_t]$	W_t	D_t	M_t^-	M_t^+	S_t^*	W_t	D_t	M_t^-	M_t^+	S_t^*
5	0.5	0.11	0.935	0.883	0.798	0.909	0.792	1	1	0.997	1	0.932
10	0.5	0.11	0.929	0.870	0.781	0.899	0.704	1	1	0.998	1	0.790
15	0.5	0.11	0.928	0.868	0.773	0.898	0.614	1	1	0.997	1	0.649
10	0.1	0.11	0.925	0.864	0.773	0.894	0.702	1	1	0.997	1	0.787
10	0.9	0.11	0.942	0.882	0.780	0.914	0.601	1	1	0.997	1	0.719
10	0.5	0.03	0.900	0.779	0.698	0.826	0.653	0.952	0.926	0.914	0.934	0.706
10	0.5	0.21	0.944	0.929	0.840	0.941	0.730	0.999	0.992	0.978	0.996	0.771

Table 20: AUC for DDSCSBM with 33 Anomalous Nodes and OR from 1 to 2.5.

Settings			Binary					Count				
CPL	ϕ	$E[W_t]$	W_t	D_t	M_t^-	M_t^+	S_t^*	W_t	D_t	M_t^-	M_t^+	S_t^*
5	0.5	0.11	0.982	0.861	0.772	0.915	0.822	0.987	0.898	0.831	0.936	0.820
10	0.5	0.11	0.980	0.853	0.763	0.909	0.702	0.988	0.899	0.833	0.937	0.705
15	0.5	0.11	0.977	0.867	0.781	0.916	0.588	0.986	0.899	0.835	0.936	0.608
10	0.1	0.11	0.973	0.868	0.789	0.916	0.716	0.982	0.903	0.847	0.937	0.704
10	0.9	0.11	0.975	0.880	0.804	0.925	0.664	0.983	0.911	0.855	0.943	0.664
10	0.5	0.03	0.884	0.752	0.691	0.805	0.642	0.897	0.763	0.705	0.814	0.656
10	0.5	0.21	0.992	0.887	0.777	0.943	0.717	0.998	0.952	0.901	0.976	0.716

Table 21: AUC for DDSCSBM with 72 Anomalous Nodes and OR from 1 to 1.5.

Settings			Binary					Count				
CPL	ϕ	$E[W_t]$	W_t	D_t	M_t^-	M_t^+	S_t^*	W_t	D_t	M_t^-	M_t^+	S_t^*
5	0.5	0.11	1	0.923	0.776	0.977	0.870	1	0.935	0.812	0.978	0.873
10	0.5	0.11	1	0.925	0.781	0.976	0.729	1	0.928	0.806	0.975	0.732
15	0.5	0.11	1	0.924	0.776	0.976	0.616	1	0.929	0.808	0.975	0.621
10	0.1	0.11	1	0.930	0.801	0.978	0.757	1	0.932	0.823	0.975	0.769
10	0.9	0.11	1	0.931	0.799	0.977	0.700	1	0.941	0.837	0.980	0.704
10	0.5	0.03	0.981	0.807	0.708	0.878	0.698	0.976	0.809	0.718	0.874	0.693
10	0.5	0.21	1	0.950	0.768	0.992	0.727	1	0.966	0.858	0.993	0.728

AUC results are reported in Tables 22 and 23 below for the gradual change in odds ratio.

Table 22: AUC for DLSCM with 39 Anomalous Nodes with $OR \in [1, 12]$.

Settings			Binary					Count				
CPL	ϕ	$E[W_t]$	W_t	D_t	M_t^-	M_t^+	S_t^*	W_t	D_t	M_t^-	M_t^+	S_t^*
15	0.5	0.11	0.786	0.814	0.794	0.817	0.617	0.941	0.947	0.942	0.949	0.793
20	0.5	0.11	0.782	0.809	0.790	0.812	0.600	0.937	0.947	0.943	0.949	0.758
25	0.5	0.11	0.779	0.805	0.786	0.808	0.560	0.936	0.942	0.938	0.945	0.722
20	0.1	0.11	0.784	0.812	0.793	0.815	0.604	0.935	0.943	0.939	0.945	0.754
20	0.9	0.11	0.782	0.810	0.792	0.812	0.560	0.940	0.948	0.943	0.950	0.715
20	0.5	0.03	0.760	0.719	0.684	0.741	0.576	0.871	0.882	0.878	0.886	0.715
20	0.5	0.21	0.791	0.862	0.861	0.848	0.605	0.952	0.963	0.959	0.964	0.767

Table 23: AUC for DDCSBM with 39 Anomalous Nodes with $OR \in [1, 3.5]$.

Settings			Binary					Count				
CPL	ϕ	$E[W_t]$	W_t	D_t	M_t^-	M_t^+	S_t^*	W_t	D_t	M_t^-	M_t^+	S_t^*
15	0.5	0.11	0.949	0.869	0.803	0.902	0.763	0.952	0.879	0.829	0.905	0.771
20	0.5	0.11	0.947	0.865	0.795	0.900	0.715	0.949	0.872	0.821	0.899	0.725
25	0.5	0.11	0.944	0.857	0.786	0.893	0.681	0.944	0.873	0.823	0.900	0.692
20	0.1	0.11	0.938	0.860	0.799	0.892	0.717	0.945	0.878	0.836	0.901	0.730
20	0.9	0.11	0.940	0.868	0.809	0.897	0.677	0.946	0.887	0.847	0.909	0.697
20	0.5	0.03	0.888	0.787	0.733	0.828	0.670	0.885	0.793	0.743	0.830	0.677
20	0.5	0.21	0.959	0.885	0.803	0.920	0.741	0.962	0.902	0.858	0.925	0.759

A.4 AUC Results for Section 4.5

Results of 200 simulations with $n = 100$, $T = 110$, and $CPL = 5, 10$, or 15 are summarized in Tables 24 - 27 using AUC.

Table 24: AUC for DLSP from $r_i = 0.1$ to $r_i = 0.020$ (B); 0.04 (C) for $N = 15$.

Settings			Binary					Count				
CPL	ϕ	$E[W_t]$	W_t	D_t	M_t^-	M_t^+	S_t^*	W_t	D_t	M_t^-	M_t^+	S_t^*
5	0.5	0.11	0.324	0.931	0.982	0.853	0.508	0.069	0.874	0.931	0.801	0.439
10	0.5	0.11	0.337	0.931	0.980	0.859	0.496	0.068	0.877	0.934	0.805	0.480
15	0.5	0.11	0.323	0.929	0.981	0.853	0.494	0.069	0.875	0.933	0.805	0.524
10	0.1	0.11	0.327	0.930	0.981	0.856	0.505	0.068	0.882	0.939	0.811	0.473
10	0.9	0.11	0.322	0.926	0.980	0.850	0.507	0.063	0.879	0.937	0.806	0.501
10	0.5	0.03	0.395	0.805	0.855	0.760	0.510	0.195	0.663	0.705	0.625	0.563
10	0.5	0.21	0.277	0.953	0.997	0.849	0.494	0.027	0.942	0.983	0.864	0.447

Table 25: AUC for DLSP from $r_i = 0.1$ to $r_i = 0.015$ (B); 0.0225 (C) for $N = 35$.

Settings			Binary					Count				
CPL	ϕ	$E[W_t]$	W_t	D_t	M_t^-	M_t^+	S_t^*	W_t	D_t	M_t^-	M_t^+	S_t^*
5	0.5	0.11	0.348	0.827	0.924	0.733	0.485	0.194	0.795	0.860	0.729	0.474
10	0.5	0.11	0.364	0.839	0.929	0.749	0.501	0.209	0.812	0.871	0.747	0.517
15	0.5	0.11	0.369	0.835	0.927	0.747	0.491	0.209	0.805	0.867	0.740	0.574
10	0.1	0.11	0.362	0.835	0.928	0.745	0.499	0.209	0.805	0.866	0.741	0.511
10	0.9	0.11	0.362	0.845	0.934	0.756	0.478	0.193	0.803	0.866	0.737	0.521
10	0.5	0.03	0.413	0.718	0.771	0.674	0.502	0.307	0.623	0.653	0.595	0.530
10	0.5	0.21	0.311	0.869	0.980	0.734	0.502	0.134	0.862	0.933	0.774	0.484

Table 26: AUC for DDCSBM from $C = 1$ to $C = 2.25$ in $C \cdot \Theta$ for $N = 15$.

Settings			Binary					Count				
CPL	ϕ	$E[W_t]$	W_t	D_t	M_t^-	M_t^+	S_t^*	W_t	D_t	M_t^-	M_t^+	S_t^*
5	0.5	0.11	0.349	0.920	0.931	0.907	0.512	0.438	0.932	0.938	0.925	0.525
10	0.5	0.11	0.351	0.929	0.939	0.914	0.483	0.422	0.938	0.945	0.929	0.496
15	0.5	0.11	0.337	0.928	0.939	0.914	0.469	0.434	0.944	0.951	0.936	0.482
10	0.1	0.11	0.343	0.932	0.940	0.919	0.502	0.434	0.944	0.949	0.938	0.503
10	0.9	0.11	0.330	0.930	0.941	0.915	0.476	0.433	0.942	0.947	0.935	0.483
10	0.5	0.03	0.473	0.779	0.798	0.761	0.508	0.481	0.780	0.798	0.762	0.517
10	0.5	0.21	0.199	0.952	0.960	0.938	0.468	0.381	0.963	0.966	0.960	0.483

Table 27: AUC for DDCSBM from $C = 1$ to $C = 1.75$ in $C \cdot \Theta$ for $N = 35$.

Settings			Binary					Count				
CPL	ϕ	$E[W_t]$	W_t	D_t	M_t^-	M_t^+	S_t^*	W_t	D_t	M_t^-	M_t^+	S_t^*
5	0.5	0.11	0.416	0.799	0.818	0.777	0.537	0.465	0.814	0.828	0.798	0.548
10	0.5	0.11	0.403	0.802	0.823	0.777	0.506	0.453	0.817	0.832	0.800	0.506
15	0.5	0.11	0.407	0.801	0.821	0.777	0.492	0.455	0.821	0.836	0.804	0.491
10	0.1	0.11	0.406	0.811	0.831	0.788	0.518	0.452	0.833	0.847	0.817	0.524
10	0.9	0.11	0.398	0.827	0.849	0.802	0.493	0.464	0.843	0.857	0.826	0.507
10	0.5	0.03	0.474	0.662	0.679	0.646	0.514	0.484	0.666	0.681	0.651	0.507
10	0.5	0.21	0.292	0.845	0.871	0.809	0.490	0.416	0.886	0.898	0.870	0.522

Results using AUC are shown in Tables 28 and 29 below for a gradual change in expected degree.

Table 28: AUC for DLSDM from $r_i \in [1/n, 4/n]$ for $N = 20$.

Settings			Binary					Count				
CPL	ϕ	$E[W_t]$	W_t	D_t	M_t^-	M_t^+	S_t^*	W_t	D_t	M_t^-	M_t^+	S_t^*
15	0.5	0.11	0.156	0.835	0.951	0.636	0.394	0.260	0.776	0.820	0.726	0.473
20	0.5	0.11	0.155	0.838	0.950	0.633	0.356	0.256	0.770	0.814	0.719	0.447
25	0.5	0.11	0.163	0.836	0.945	0.640	0.318	0.260	0.772	0.816	0.724	0.430
20	0.1	0.11	0.160	0.839	0.949	0.638	0.351	0.263	0.772	0.816	0.724	0.448
20	0.9	0.11	0.153	0.835	0.946	0.634	0.359	0.254	0.770	0.813	0.720	0.462
20	0.5	0.03	0.217	0.840	0.887	0.775	0.455	0.350	0.611	0.635	0.590	0.475
20	0.5	0.21	0.131	0.704	0.965	0.467	0.293	0.213	0.827	0.873	0.765	0.411

Table 29: AUC for DDCSBM from $C \in [1, 5]$ in $C \cdot \Theta$ for $N = 35$.

Settings			Binary					Count				
CPL	ϕ	$E[W_t]$	W_t	D_t	M_t^-	M_t^+	S_t^*	W_t	D_t	M_t^-	M_t^+	S_t^*
15	0.5	0.11	0.219	0.900	0.906	0.891	0.593	0.354	0.902	0.905	0.898	0.653
20	0.5	0.11	0.228	0.904	0.910	0.897	0.521	0.347	0.910	0.913	0.906	0.580
25	0.5	0.11	0.225	0.908	0.913	0.900	0.464	0.348	0.912	0.916	0.907	0.524
20	0.1	0.11	0.216	0.902	0.907	0.893	0.508	0.336	0.913	0.917	0.909	0.583
20	0.9	0.11	0.219	0.906	0.912	0.897	0.531	0.336	0.908	0.911	0.904	0.579
20	0.5	0.03	0.420	0.832	0.846	0.818	0.569	0.446	0.838	0.849	0.826	0.594
20	0.5	0.21	0.132	0.922	0.928	0.911	0.441	0.249	0.925	0.928	0.921	0.548

References

- Adamic, L. A. and Glance, N. “The political blogosphere and the 2004 US election: divided they blog.” In *Proceedings of the 3rd International Workshop on Link Discovery*, 36–43. ACM (2005).
- Azarnoush, B., Paynabar, K., Bekki, J., and Runger, G. “Monitoring temporal homogeneity in attributed network streams.” *Journal of Quality Technology*, 48(1):28–43 (2016).
- Bassett, D. S. and Bullmore, E. “Small-world brain networks.” *The Neuroscientist*, 12(6):512–523 (2006).
- Box, G., Jenkins, G., and Reinsel, G. “Time series analysis: forecasting and control, 4th edn. John Wiley & Sons.” *Inc, UK* (2008).
- Hidalgo, C. A., Blumm, N., Barabási, A.-L., and Christakis, N. A. “A dynamic network approach for the study of human phenotypes.” *PLoS computational biology*, 5(4):e1000353 (2009).
- Hoff, P. D., Raftery, A. E., and Handcock, M. S. “Latent space approaches to social network analysis.” *Journal of the American Statistical Association*, 97(460):1090–1098 (2002).
- Huberman, B. A. and Adamic, L. A. “Internet: growth dynamics of the World-Wide Web.” *Nature*, 401:131 (1999).
- Jardim, F. S., Chakraborti, S., and Epprecht, E. K. “Two perspectives for designing a phase II control chart with estimated parameters: The case of the Shewhart Chart.” *Journal of Quality Technology*, 1–20 (2019).
- Karrer, B. and Newman, M. E. “Stochastic blockmodels and community structure in networks.” *Physical review E*, 83(1):016107 (2011).
- Kim, B., Lee, K. H., Xue, L., Niu, X., et al. “A review of dynamic network models with latent variables.” *Statistics Surveys*, 12:105–135 (2018).
- Lynall, M.-E., Bassett, D. S., Kerwin, R., McKenna, P. J., Kitzbichler, M., Muller, U., and Bullmore, E. “Functional connectivity and brain networks in schizophrenia.” *Journal of Neuroscience*, 30(28):9477–9487 (2010).
- Matias, C. and Miele, V. “Statistical clustering of temporal networks through a dynamic stochastic block model.” *Journal of the Royal Statistical Society: Series B (Statistical Methodology)*, 79(4):1119–1141 (2017).
- Milgram, S. “The small world problem.” *Psychology Today*, 2:60–67 (1967).
- Montgomery, D. C. *Introduction to statistical quality control*. John Wiley & Sons (2007).
- Pagani, G. A. and Aiello, M. “The power grid as a complex network: a survey.” *Physica A: Statistical Mechanics and its Applications*, 392(11):2688–2700 (2013).
- Priebe, C. E., Conroy, J. M., Marchette, D. J., and Park, Y. “Scan statistics on Enron graphs.” *Computational & Mathematical Organization Theory*, 11(3):229–247 (2005).

- Savage, D., Zhang, X., Yu, X., Chou, P., and Wang, Q. “Anomaly detection in online social networks.” *Social Networks*, 39:62 – 70 (2014).
URL <http://www.sciencedirect.com/science/article/pii/S0378873314000331>
- Sengupta, S. and Woodall, W. H. “Discussion of “Statistical Methods for Network Surveillance” by D. R. Jeske, N.T. Stevens, A. G. Tartakovsky and J. D. Wilson.” *Applied Stochastic Models in Business and Industry*, 34(4):446–448 (2018).
- Sewell, D. K. and Chen, Y. “Latent Space Models for Dynamic Networks.” *Journal of the American Statistical Association*, 110(512):1646–1657 (2015).
- . “Latent space models for dynamic networks with weighted edges.” *Social Networks*, 44:105–116 (2016).
- Snijders, T. A. and Nowicki, K. “Estimation and prediction for stochastic blockmodels for graphs with latent block structure.” *Journal of classification*, 14(1):75–100 (1997).
- Wilson, J. D., Stevens, N. T., and Woodall, W. H. “Modeling and detecting change in temporal networks via a dynamic degree corrected stochastic block model.” *QREI*, 35:1363–1378 (2019).
- Woodall, W. H., Zhao, M. J., Paynabar, K., Sparks, R., and Wilson, J. D. “An overview and perspective on social network monitoring.” *IISE Transactions*, 49(3):354–365 (2017).
- Xia, M., Wang, J., and He, Y. “BrainNet Viewer: a network visualization tool for human brain connectomics.” *PLOS One*, 8(7):e68910 (2013).
- Yu, L., Woodall, W. H., and Tsui, K.-L. “Detecting node propensity changes in the dynamic degree corrected stochastic block model.” *Social Networks*, 54:209–227 (2018).
- Zabelina, D. L. and Andrews-Hanna, J. R. “Dynamic network interactions supporting internally-oriented cognition.” *Current opinion in neurobiology*, 40:86–93 (2016).
- Zhao, M. J., Driscoll, A. R., Sengupta, S., Fricker Jr, R. D., Spitzner, D. J., and Woodall, W. H. “Performance evaluation of social network anomaly detection using a moving window-based scan method.” *Quality and Reliability Engineering International*, 34(8):1699–1716 (2018a).
- Zhao, M. J., Driscoll, A. R., Sengupta, S., Stevens, N. T., Fricker Jr, R. D., and Woodall, W. H. “The effect of temporal aggregation level in social network monitoring.” *PloS One*, 13(12):e0209075 (2018b).